Geological Sciences Department Senior Thesis

A thesis submitted in partial fulfillment of the requirements for the degree of Bachelors of Science in Geological Sciences.

STRUCTURAL ANALYSIS OF THE BORREGO SPRINGS SHEAR ZONE; IMPERIAL COUNTY, CALIFORNIA.

By:

Kayla A. Kroll

STRUCTURAL ANALYSIS OF THE BORREGO SPRINGS SHEAR ZONE, IMPERIAL COUNTY CALIFORNIA.

By:

Kayla A. Kroll

Geological Sciences Department

California State Polytechnic University,

Pomona, CA

Senior Thesis

Submitted in partial fulfillment

Of the requirements for the

B.S. in Geological Science

TABLE OF CONTENTS

ABSTRACT

The Borrego Springs Shear Zone (BSSZ) is located in the Peninsular Ranges batholith ~35 miles west of the Salton Sea, Imperial Valley California. In general, this part of the batholith is composed of granodiorites and tonalites. The shear zone formed as a result of westward directed thrusting of the Eastern Peninsular Range block over the western block during the Laramide orogeny under lower amphibolite / upper greenschist facies metamorphism. Mylonites of the BSSZ experienced unique deformation patterns and varied amounts of shear strain.

Three years of Structural Geology classes mapped the orientation of undeformed and deformed pegmatite dikes, S and C planes, xenoliths in host tonalite, and mylonitic lineation. I collected additional data during December 2007 using a Bruton and positioned with a Magellan Mobilemapper. These data were mapped using ArcGIS software and analyzed with stereonets. Also, orientations of S and C planes and aspect ratios were measured from twelve thin sections and mathematically and statistically analyzed.

Preliminary field observations support the hypothesis that the BSSZ was deformed under simple shearing conditions. Upon analysis, I found that the samples fit within the error bounds of the simple shear model, but that shear strain is heterogeneous and with identifiable zones of high and low strain. Additionally, individual mineral behavior is also heterogeneous and grain-shape data does not convincingly fit the simple shear model. Three dimensional grain-shape analysis suggests a significant flattening component of strain during deformation. Analysis at the macroscopic and microscopic scales also produces a range of shear strain values, therefore it can not be said which scale provides the best estimate of true strain.

INTRODUCTION

Purpose

East of Borrego Springs, Ca I studied the geometry and lateral variations of strain within the exposed shear zone. The goal of this study was to understand the nature of deformation within the Borrego Springs Shear Zone. Through analysis of nearly five hundred data points, I was able to address an important question: *To what degree do the mylonites of the Borrego Springs Shear Zone approximate simple shear deformation?* My research directly addresses the hypothesis that the Borrego Springs Shear zone was deformed under simple shear conditions. Figure 1 depicts a Simple Shear Model identifying two important features that will change as shearing progresses: 1) The original grain shape will become more elongate as represented by the initial sphere becoming more elliptical, and 2) The angle of the S-plane relative to the shear zone boundary, or C-plane, will decrease as shearing increases. If I can prove simple shear deformation, I will be able to conduct my analysis in two dimensions as opposed to a more complicated three dimensional analysis.

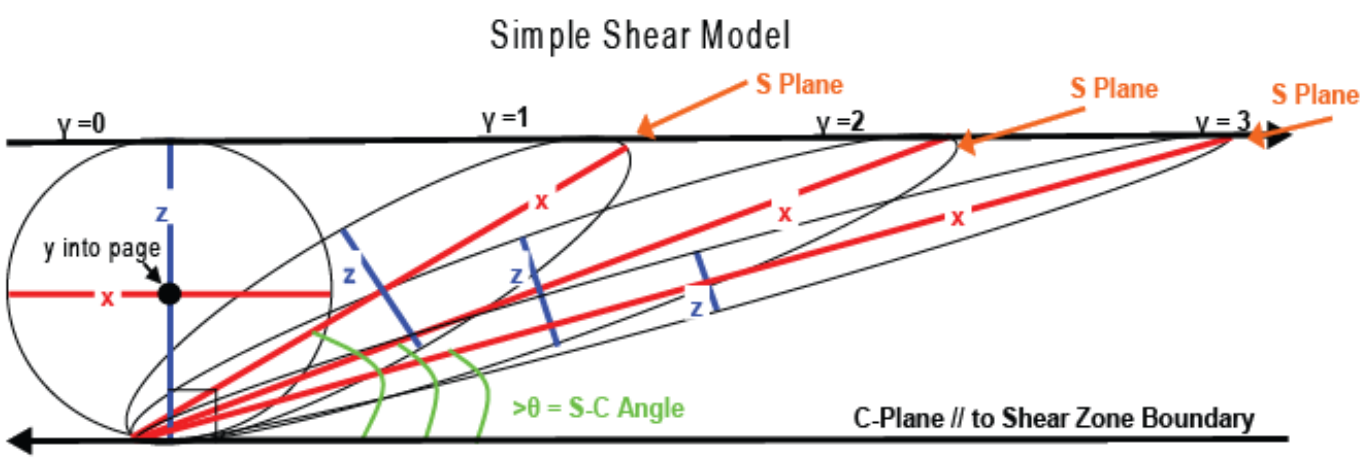

Figure 1: Depicts the particle motion expected during simple shear. According to this model, original grain shape will become more elongate and the S-C angle will decrease as shear strain increases.

Objectives

I carried out this investigation over the course of one year. My main objectives were to combine previous research, structural field studies, and strain analysis to test the simple shear hypothesis stated earlier.

Review of published papers and text provide the basis for geologic and tectonic history, age dates of batholithic rocks, and preliminary results of structural and shear strain analysis. Field measurements which have been collected in recent years by structural geology students are compiled, mapped, and analyzed with the addition of new data collected for the sole purpose of extending this investigation.

GPS units, Brunton compasses and topographic maps are the primary tools used at the macroscopic scale to collect data. These field measurements include the orientation of average S and C plane foliations measured in the field at the macroscopic scale, lineations, orientation of deformed and undeformed pegmatite dikes, and undeformed xenoliths. I incorporated this data in geologic maps of the study area which are spatially referenced using GIS software, used in stereo net analysis and analyzed to demonstrate variations (if any) between relative scales of this project.

I collected additional data at the microscopic (thin section) scale and which includes the orientation of S and C planes for use in shear strain analysis, and aspect ratios of prominent mineral species. I interpreted this data using existing mathematical functions that relate the S-C angle (θ) to shear strain values (γ) as described by Davis and Reynolds (1996) and previously employed by Nourse (1989). Furthermore, I completed statistical analysis that includes the approximate error of collected data, and variation from the predicted results. I compared these data with the Simple Shear model in order to address the on hypothesis. Various supporting graphs, histograms and plots are presented.

GEOLOGIC SETTING

The Borrego Springs Shear Zone (BSSZ) lies west of the city Borrego Springs, Imperial County, California. The study site of this project lies within the Anza Borrego State Park along Montezuma Valley Road, highway S22. The shear zone lies at the center of two splays of the southern San Andreas Fault system, south to southwest of the San Jacinto Fault and east of the Elsinore Fault. Both these faults are of younger age than the BSSZ. A map of the BSSZ and the local vicinity is shown in Figure 2a.

Figure 2a: Google Earth regional map showing the study area outlined in red box, approximately 35 miles west of the Salton Sea.

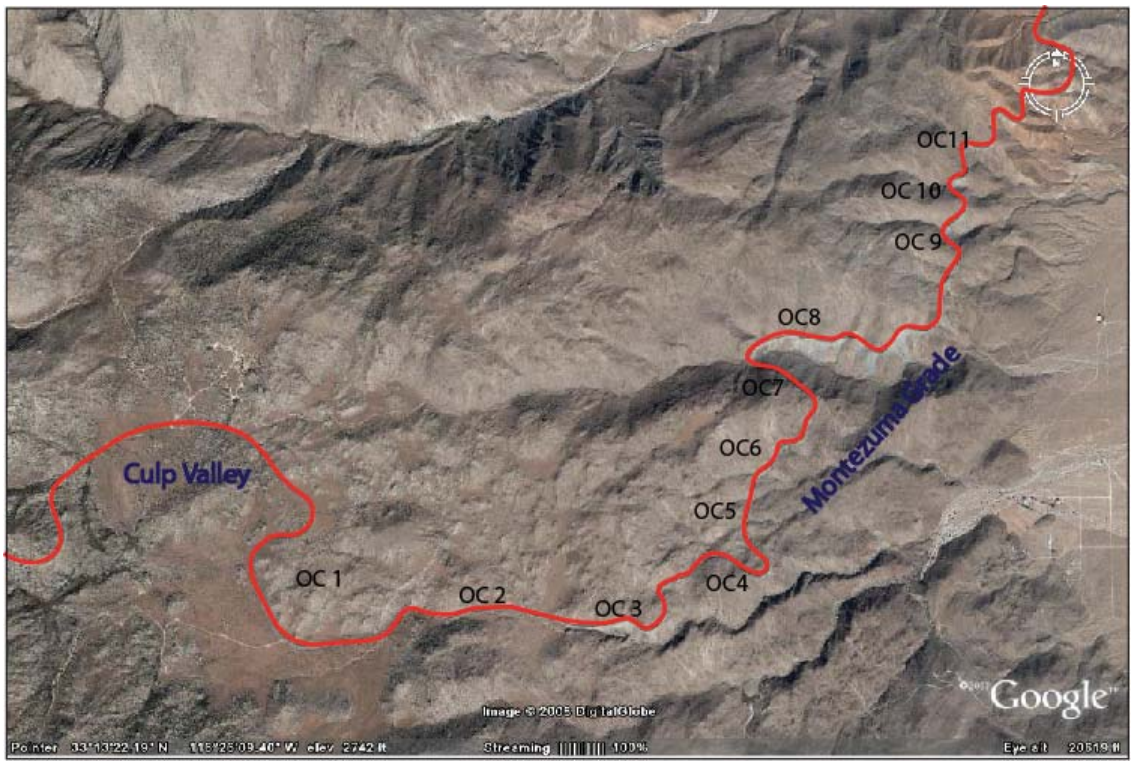

Figure 2b: Google Earth image of study area expanded from red box in Fig 2a. Image shows GSC333 focus near Culp Valley and my field work along Montezuma Grade at outcrops (OC) 1-11.

Regionally, the BSSZ lies on the eastern edge of the Peninsular Ranges batholith. The batholith consists of Cretaceous Calc-Alkaline plutons intruded into Triassic and Jurassic metasedimentary host rock (English, 2003). The Western Peninsular Range intrusions have been dated at 126-105 Ma and the Eastern at 105-90 Ma. Uplift and metamorphism of the batholith is associated with the Laramide Orogeny as a result of shallowing westward subduction of the Farallon Plate beneath the North American Plate (Wetmore, 2003). As the angle of subduction decreased it is thought that uplift swept through the western United States with older compressional structures located in southern California and younger rocks occurring as far east as Wyoming.

The protolith tonalite of the BSSZ, sampled from Montezuma Grade yielded a $^{206}Pb/^{238}U$ date of ~92MA (Silver, 1991). In outcrop, the deformation zone begins just westward to the Montezume grade and is overlain by the metasedimentary host rock eastward, near the bottom of the grade. The shear zone outcrops vertical distances greater than 1500 feet and ~8300 feet horizontally in map view. It records uplift of the Eastern Peninsular Range over the Western Peninsular Range which coincides with the top to the

west sense of shear expressed in the foliated fabric of the mylonitic tonalite (Simpson, 1984a).

From thin section analysis during this project, it has been confirmed that the BSSZ experienced lower amphibolite / upper greenschist facies metamorphism. This is demonstrated by the brittle behavior of the feldspar and plagioclase grains. Also, biotite and hornblende are sheared and recrystallized, but are only locally replaced by chlorite. However, quartz grains in all the sections have been strung out into recrystallized ribbons which suggests ductile flow. At upper greenschist / lower amphibolite conditions, it can be concluded that deformation occurred near the brittle/ductile transition (Simpson, 1984b). Thus the area nicely exposes an exhumed portion of the brittle/ductile transition.

Figure 3: Sample KK102 depicting S planes highlighted in yellow, C planes highlighted in blue, quartz grains outlined in red, and feldspar grain outlined in green.

The C- planes or shear planes of the mylonitic tonalite (Figure 3) are aligned approximately parallel to the boundaries of the shear zone. The foliation planes or S-planes are aligned at some angle relative to the boundaries of the shear zone which is a consequence of the amount of strain.

PREVIOUS STUDIES

The Eastern Peninsular Range Mylonite Zone (EPRMZ) covers a much broader strike length and has been previously studied by Sharp (1979)[1] Simpson (1984)[2]. [2]Simpson's research focused on macroscopic structural evidence for east over west sense of shear collected in the field from road cuts along Montezuma Highway. Thin sections cut perpendicular to foliation and parallel to lineation microscopically supported this sense of shear. [1]Sharp (1979) suggests that deformation in this area occurred due to west directed thrusting of the Eastern Peninsular Range over the Western Peninsular Range as a response to closure of the back-arc basin inland of east-dipping subduction of the Farallon Plate. Simpson suggests that the EPRMZ was deformed during upper greenschist / lower amphibolite facies metamorphism with shear strain (γ) values between 2 and 4.

My research conducted in the Borrego Springs Shear Zone (BSSZ) builds on collaborative effort. For three years, Geological Science students at California State Polytechnic University, Pomona have been conducting field work in the Anza Borrego Desert, as a part of the fall quarter Structural Geology class (GSC 333) led by Dr. Jon Nourse. The majority of this work focused on the area surrounding Culp Valley and smaller portions along the Montezuma Valley Road Grade, Highway S22, Imperial County, California.

Students of the GSC 333 used Garmin GPSMAP60 for UTM coordinates, Brunton Compasses, topographic and geologic maps to collect data. Measurements included orientation of undeformed pegmatite dikes and xenoliths within the undeformed tonalite, north and south of Culp Valley. Nearing the Montezuma Grade, orientations of average S and C planes, lineations and S-plane parallel dikes were measured in macroscopic outcrop scale. These data were compiled by Julie Brown and used to create geologic maps in Adobe Illustrator. Analysis of stereonets was performed using Allmendinger's StereoWin program to show the preferred orientation of all the data.

The GSC 333 data demonstrate three dominant orientations of undeformed pegmatite dikes west of Culp Valley in the undeformed tonalite host rock: N3W/57SW, N23E/65NW, and N70E/73NW. Moving into the shear zone, students recognized "S" and

"C" foliations in outcrop and confirmed a top-to-the-west sense of shear. Stereonet analysis of measurements along Montezuma grade shows S and C plane average orientation to be N5E/35SE and N12E/22SE, respectively. In this area, average deformed pegmatite dike orientations were found to generally trend N9W/32NE suggesting rotation of the original west dipping dike sets into the S plane foliation. The mylonitic tonalite in this area show lineations that are oriented on average ~N77E/34. I compiled the GSC 333 data with the additional measurements collected in December 2007 for use in my investigation.

METHODS AND PROCEDURE

During December 2007, I carried out field work primarily focusing on road cut outcrops along the Montezuma Valley Road Grade and traverses of adjacent valleys and ridges. I used ArcPad software on a Magellan MobileMapper to store data collected in the field. This technological advance led to the ability to collect substantially larger amounts of data, limited the time needed for data entry, and ArcGIS software allowed mapping to be spatially referenced. I gathered over two hundred and fifty data points of the above mentioned type. I also collected oriented hand samples out of outcrops, properly documented and marked with the strike/dip of foliation and trend/plunge of lineation. Furthermore, I compiled spreadsheets of all data and new maps exemplifying class data, my data. From these data I created spatially referenced maps using ArcGIS.

I spent many hours completing laboratory work; organizing, mapping, and analyzing this vast amount of data. First, I created geologic maps depicting major rock units, strike and dip of pegmatite dikes, S and C foliation and lineation were projected using ArcGIS and further cosmetic work using Adobe Illustrator. I created a total of five maps; Figure 5 illustrates work done by three years of Structural Geology students in the Culp Valley and down Montezuma Grade. Figure 7 shows the data a personally collected, mainly along road-cut outcrops down Montezuma Grade and to a lesser extent, the Culp Valley. Next is a compilation of all the gathered data for the two areas (Figure 8). Data points along Montezuma Grade were added to a topographic map, and interpolated by nearest neighbor to show zones of high and low shear strain (Figure 18). Lastly, I overlaid Google Earth Professional satellite images over USGS topographic quadrangle maps

to show the extent of the topography and rotation of pegmatite dikes through the shear zone (Figure 19).

Secondly, twelve thin sections of the oriented hand samples were cut; four cut parallel to lineation (i.e. the YZ plane) and eight cut perpendicular to foliation (i.e. the XZ plane). The XZ sections were analyzed using a Leitz and Nikon Petrographic microscopes to determine the orientation of S and C planes. The differences of the averages of these two measurements allow for calculations of shear strain (γ) on a microscopic level. Standard deviations of these measurements were found to determine the approximate error. Additionally, both YZ and XZ sections of the same sample were analyzed to find aspect ratios in the X, Y, and Z dimension of various feldspars, plagioclase, quartz, biotite, and hornblende. These figures were used in statistical analysis of the strain ellipsoid with the ultimate goal of obtaining shear strain values. The Figure 4 shows an ellipsoid diagram and related mathematical operations.

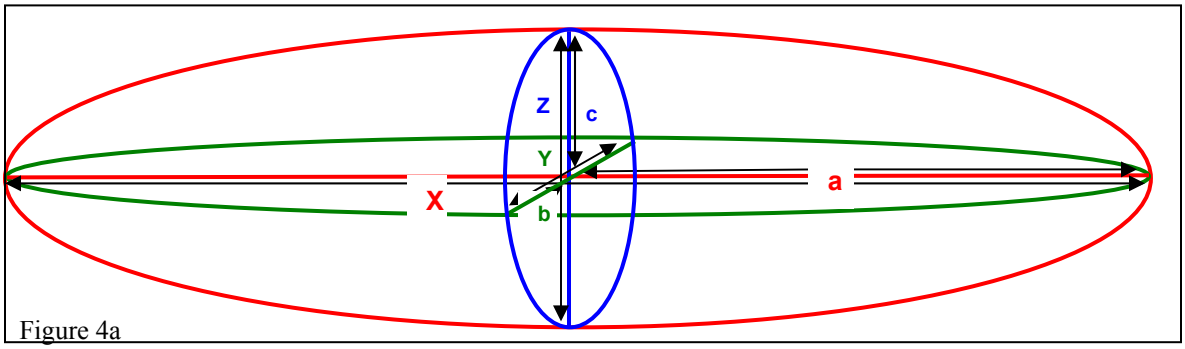

Figure 4a

Semi-Axis Lengths:

a = (1/2)X	**(Eq: 1)**
b = (1/2)Y	**(Eq: 2)**
c = (1/2)Z	**(Eq: 3)**

$r = \sqrt[3]{(a*b*c)}$

Longitudinal Strain:

In X direction (ex) = (a-r)/r	**(Eq: 4)**
In Y direction (ey) = (b-r)/r	**(Eq: 5)**
In Z direction (ez) = (c-r)/r	**(Eq: 5)**

Principle Stretches:

In X direction = 1 + ex = Sx	**(Eq: 7)**
In Y direction = 1 + ey = Sy	**(Eq: 8)**
In Z direction = 1 + ez = Sz	**(Eq: 9)**

Rxz = Sx/Sz	**(Eq: 10)**
Rxy = Sx/Sy	**(Eq: 11)**
Ryz = Sy/Sz	**(Eq: 12)**

Figure 4b

Figure 4a: Diagram of an ellipsoid depicting long dimensions and semi-axes
Figure 4b: Mathematical operations performed to calculate strain ellipsoid values

Lastly, I conducted analysis of the aspect ratios and strain ellipsoid to address the working hypothesis. Ubiquitous occurrences of L-S tectonities and S-C fabric led to the suspicion that this area was deformed in the simple shearing fashion. The measured Rxz and Ryz values provide three dimensional grain proportions after deformation, from which we can calculate the amount of strain required to create this shape and whether the deformation approximates plane strain. Plane strain deformation is a special shearing case where deformation takes place in two dimensions instead of three.

This information can further be used to extrapolate displacement caused by the shearing event and the amount of rotation within the sheared block recorded by the deformed pegmatite dikes. If this hypothesis can be proven, it would be theoretically possible assume simple shear/plane strain and to simply use the Rxz values to calculate the shear strain values where both Rxz and Ryz samples are not available. Additionally, macroscopic and microscopic measurements were compared to determine how accurate average estimates of S and C planes taken in the field compare to those found in thin sections. If these two methods are consistent, it can be assumed that thin section analysis is not required and that macroscopic analysis can provide an accurate S-C Angle and subsequent shear strain value.

DATA AND RESULTS

Macroscopic Observations

Data collected by three GSC 333 classes was compiled and I created new geologic maps and stereonet diagrams. The first of these maps (Figure 5) display all structural data collected by GSC 333 students including strike and dip of undeformed pegmatite dikes near Culp Valley, deformed and rotated pegmatite dikes along Montezuma Highway, undeformed xenoliths near Culp Valley, S plane foliation and shear planes (C-planes) of mylonitic tonalite through Montezuma grade, trend and plunge of lineations in mylonitic tonalite (Refer to Figure 5 and Plate 1).

Borrego Springs Shear Zone; GSC 333 Class Data

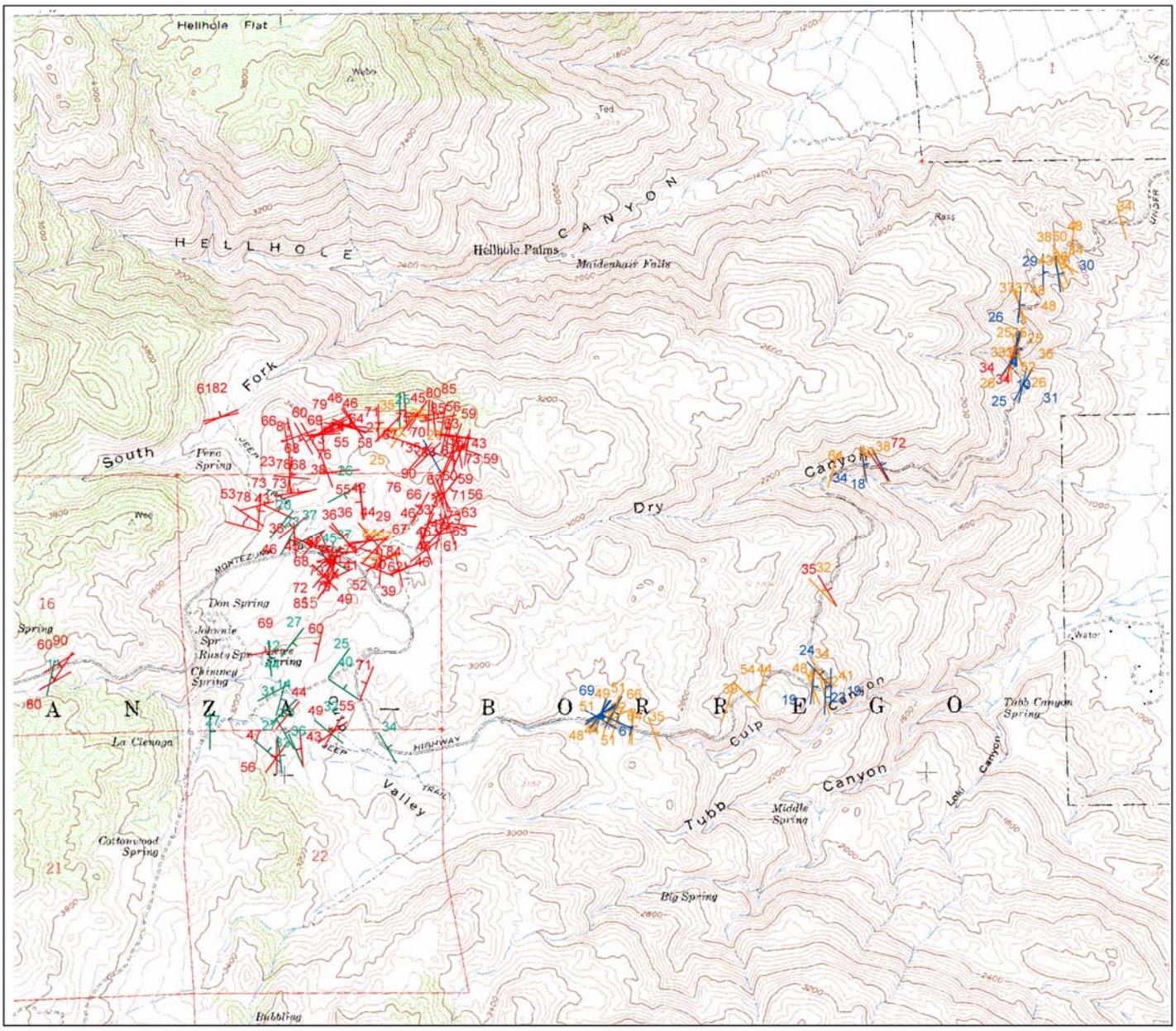

Legend

- Shear Planes (C-Planes)
- Mylonitic Foliation (S- Planes)
- Undeformed Pegmatite Dikes
- Xenoliths

N

0 250 500 1,000 Meters

Discussion

Fig 5: Portrayed in this map are the mylonitic foliations (S-Planes) and shear planes (C-Planes) that were mapped from Culp Valley and along the Montezuma Grade in through the Borrego Springs Shear Zone. These data were used to contruct stereo nets and statistically analyze the orientations of this data. C-Planes were found to average at 5.3/24.6 with S-Planes at 2.2/42.8. These planes strike approximately parallel and differ in dip by ~18 degrees. This data was used to confine the values of shear strain across the BSSZ.

Additionally, xenoliths that record the magmatic flow direction during batholithic emplacement were measured and found to trend on average at 27.0/20.8. Undeformed pegmatite dikes were measured in the area surrounding Culp Valley. Such dikes are were intruded prior to metamorphism and were subsequently rotated into parallel to folation in the shear zone. Undeformed dikes trend at: 176.8/56.1, 201.3/63.8, and 250.6/72.0

I conducted stereonet analysis from this class data and derived new averages (Figure 6A-F). Individual stereonets were created for C planes, S planes, undeformed dikes and lineations. From these plots, the average orientation of these data can be deduced. The average S and C planes (Figure 6A,B) were found to be orientated at 2.2/42.8 and 5.3/24.6 respectively (Strike measured in azimuths and dip according to right hand rule). The average trend and plunge of lineations was found to be at 78.5/37.6 (Figure 6E). In the area west of the shear zone, undeformed pegmatite dikes were found to form three orientations at 176.8/56.1, 201.3/63.8, and 250.6/72.0 (Figure 6C). Moving into the shear zone, pegmatite dikes begin to rotate parallel to foliation. Deformed dikes show averages at: 14.5/27.4 (Figure 6D). Xenoliths in the undeformed tonalite which record magmatic flow during batholith emplacement, vary significantly from this pattern and trend on average at 27.0/20.8 (Figure 6F).

The above described procedure was used to illustrate and analyze data I collected during the winter of 2007. In this case, all macroscopic field measurements were imported into ArcMap and spatially plotted over a topographic quadrangle map to create a geologic map of the study area. These maps include strike and dip of S and C planes of mylonitic tonalite measured at road cuts along Montezuma grade, a few undeformed pegmatite dikes west and east of Culp Valley, and trend and plunge of lineation of the mylonitic tonalite. Calculations were also made in the lab to determine S-C angles from collected field data at individual outcrops. Additional maps display strain value variations at outcrop scale through the shear zone (Refer to Figure 7 and Plate 2). Additionally, this data was compiled with class data to create similar structural geologic maps (Refer to Figure 8 and Plate 3)

I carried out further stereonet analysis with my data collected in December 2007. Again, average orientations of these data were obtained. The average trend of the S and C planes (Figure 9A,B) were found to be 327.3/40.5 and 343.4/26.3 respectively. Xenoliths west of Culp Valley average at: 260.3/ 37.1 (Figure 9F).Two average orientations of undeformed dikes were found from this information. These are orientated at 235.0/45.9 and 186.7/48.8 (Figure 9C). Foliated pegmatite dikes parallel to the S-Planes average at: 8.2/38.2 (Figure 9D). Lineations of the mylonitic tonalite through Montezuma grade were found to have an average trend and plunge of 149.5/50.1 (Figure 9E).

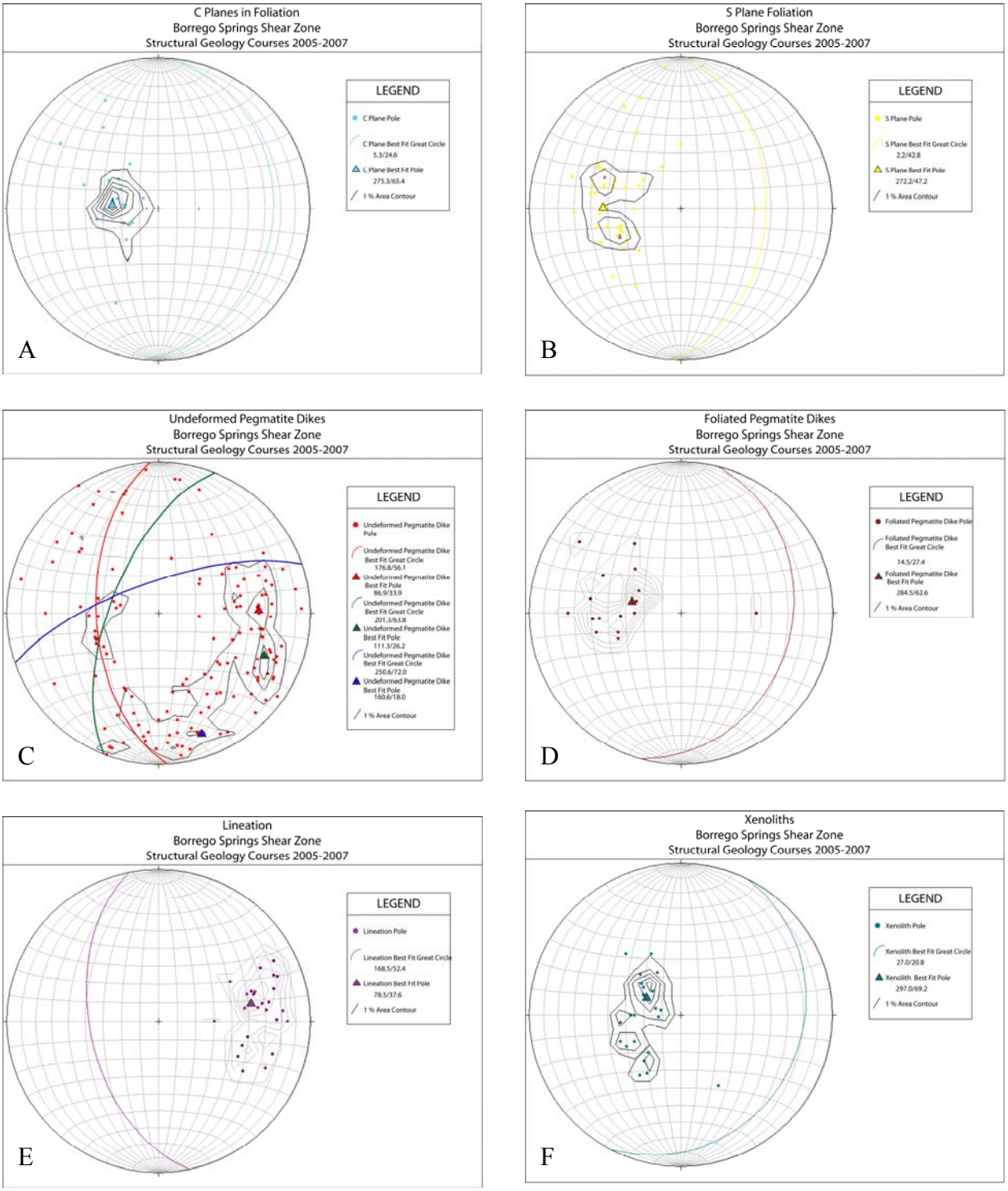

Figure 6 A-F: Stereonet diagrams of GSC 333 data. A: C-Planes, B: S-Planes, C: Undeformed pegmatite dikes, D: Foliated pegmatite dikes, E: Mylonitic Lineation, F: Xenoliths. All diagrams show best fit great circle as statistical average and best fit poles.

Borrego Springs Shear Zone; Data from December 2007

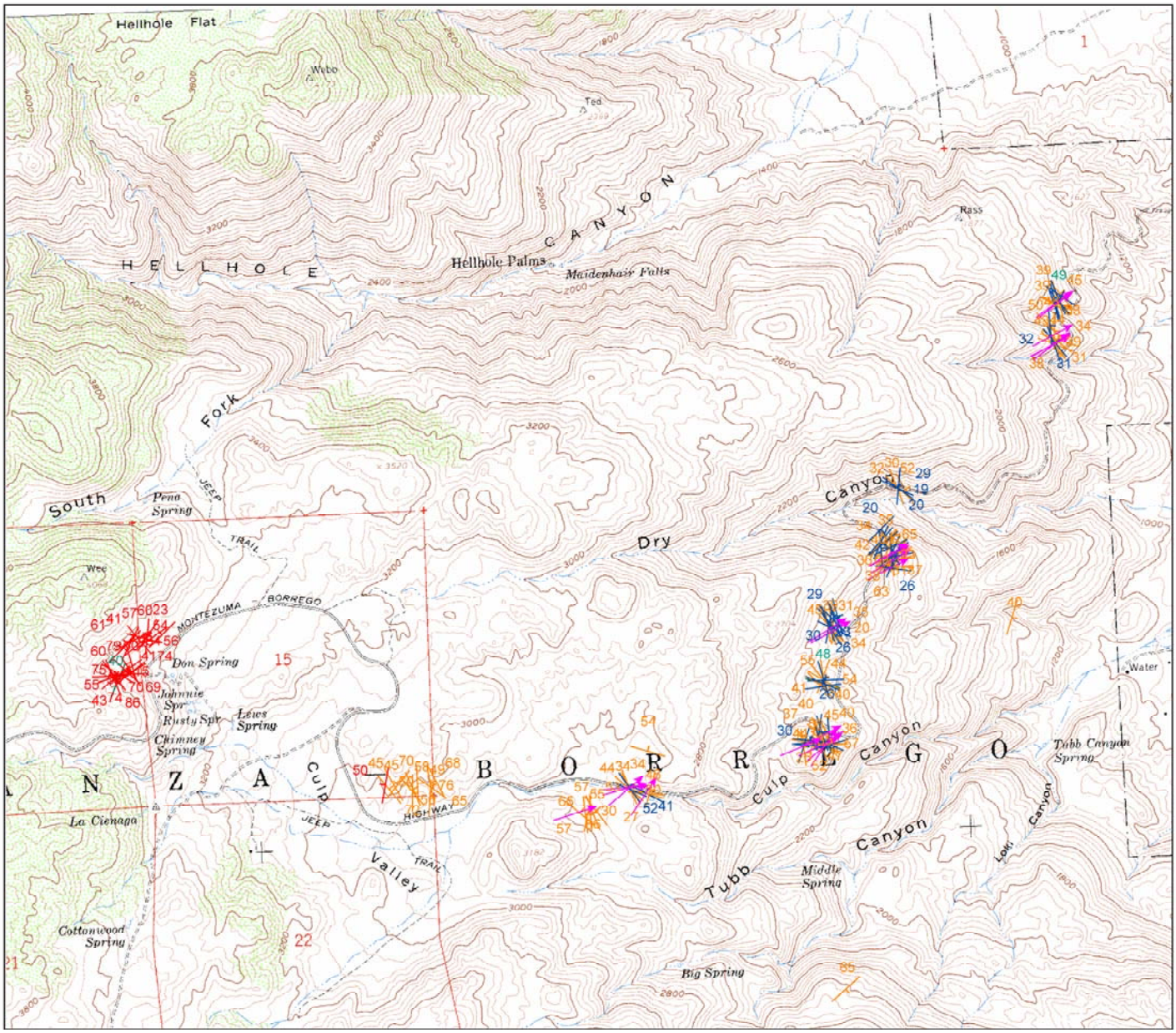

Legend

- Shear Planes (C-Planes)
- Mylonitic Foliation (S- Planes)
- Undeformed Pegmatite Dikes
- Mylonitic Lineation
- Xenoliths

0 250 500 1,000 Meters

N

Discussion

Figure 7: Portrayed in this map are the mylonitic foliations (S-Planes) and shear planes (C-Planes) that were mapped from Culp Valley and along the Montezuma Grade in through the Borrego Springs Shear Zone. These data were used to contruct stereo nets and statistically analyze the orientations of this data. C-Planes were found to average at 343.4/26.3 with S-Planes at 327.3/40.5. These planes strike approximately parallel and differ in dip by ~15degrees. This data was used to confine the values of shear strain across the BSSZ.

Additionally, xenoliths that record the magmatic flow direction during batholithic emplacement were measured and found to trend on average at 260.3/37.1. Undeformed pegmatite dikes were measured in the area surrounding Culp Valley. Such dikes are were intruded prior to metamorphism and were subsequently rotated into parallel to folation in the shear zone. Undeformed dikes trend at: 235.0/45.9,186.7/48.8. Mylonitic linetaion trend at: 59.5/39.9.

Borrego Springs Shear Zone; Compiliation of All Data

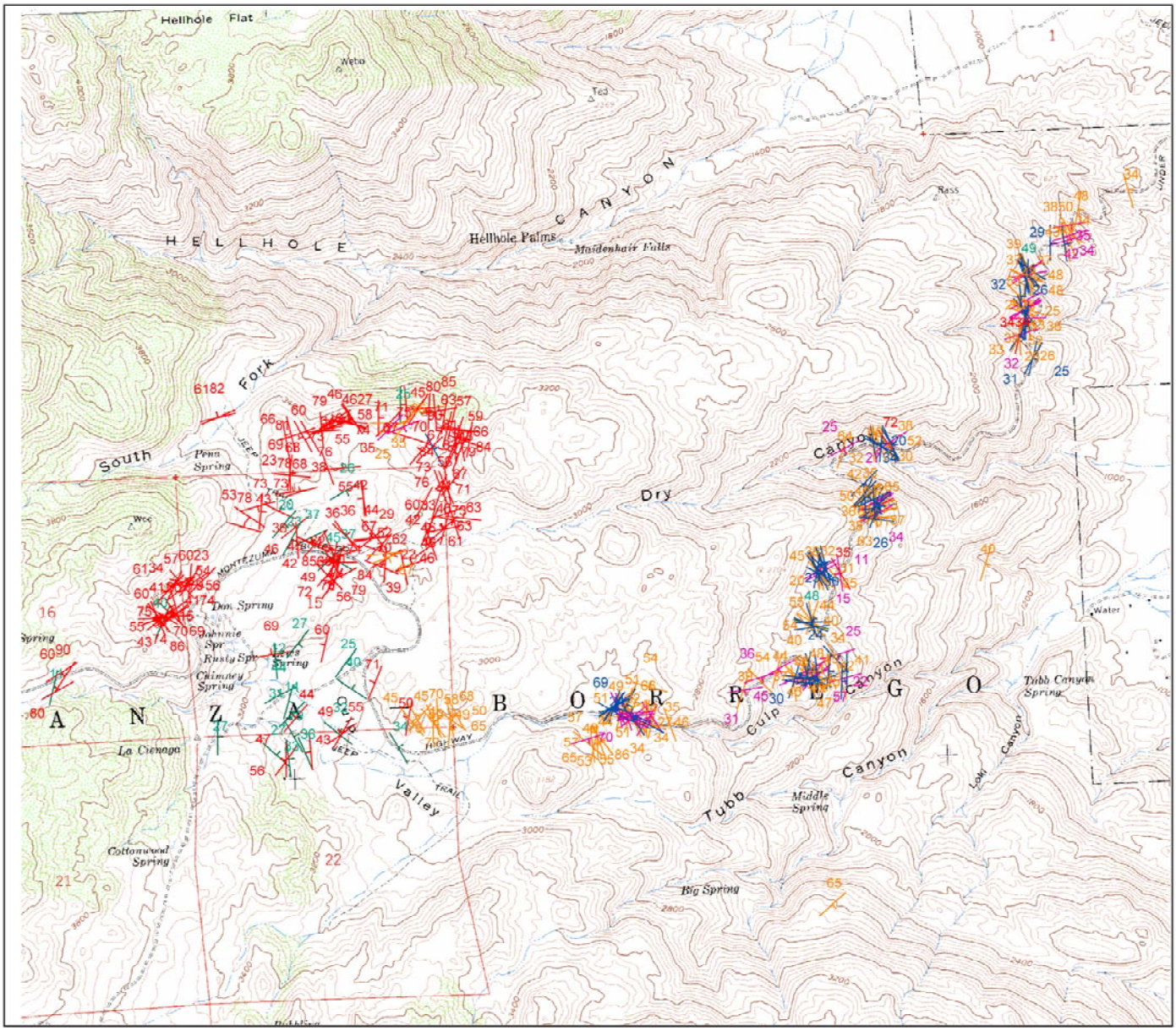

Legend

- Shear Planes (C-Planes)
- Mylonitic Foliation (S- Planes)
- Undeformed Pegmatite Dikes
- Mylonitic Lineation
- Xenoliths

0 245 490 980 Meters

N

Discussion

Figure 8: Portrayed in this map are the mylonitic foliations (S-Planes) and shear planes (C-Planes) that were mapped from Culp Valley and along the Montezuma Grade in through the Borrego Springs Shear Zone. These data were used to contruct stereo nets and statistically analyze the orientations of this data. C-Planes were found to average at 0.8/24.8 with S-Planes at 1.3/45.3. These planes strike approximately parallel and differ in dip by ~20 degrees. This data was used to confine the values of shear strain across the BSSZ.

Additionally, xenoliths that record the magmatic flow direction during batholithic emplacement were measured and found to trend on average at 27.0/20.8. Undeformed pegmatite dikes were measured in the area surrounding Culp Valley. Such dikes are were intruded prior to metamorphism and were subsequently rotated into parallel to folation in the shear zone. Undeformed dikes trend at: 45.9/61.6,178.9/51.3, 207.8/63.7, 233.3/ 52.8, 353.3/33.1. Mylonitic linetaion trend at: 68.7/ 38.2_

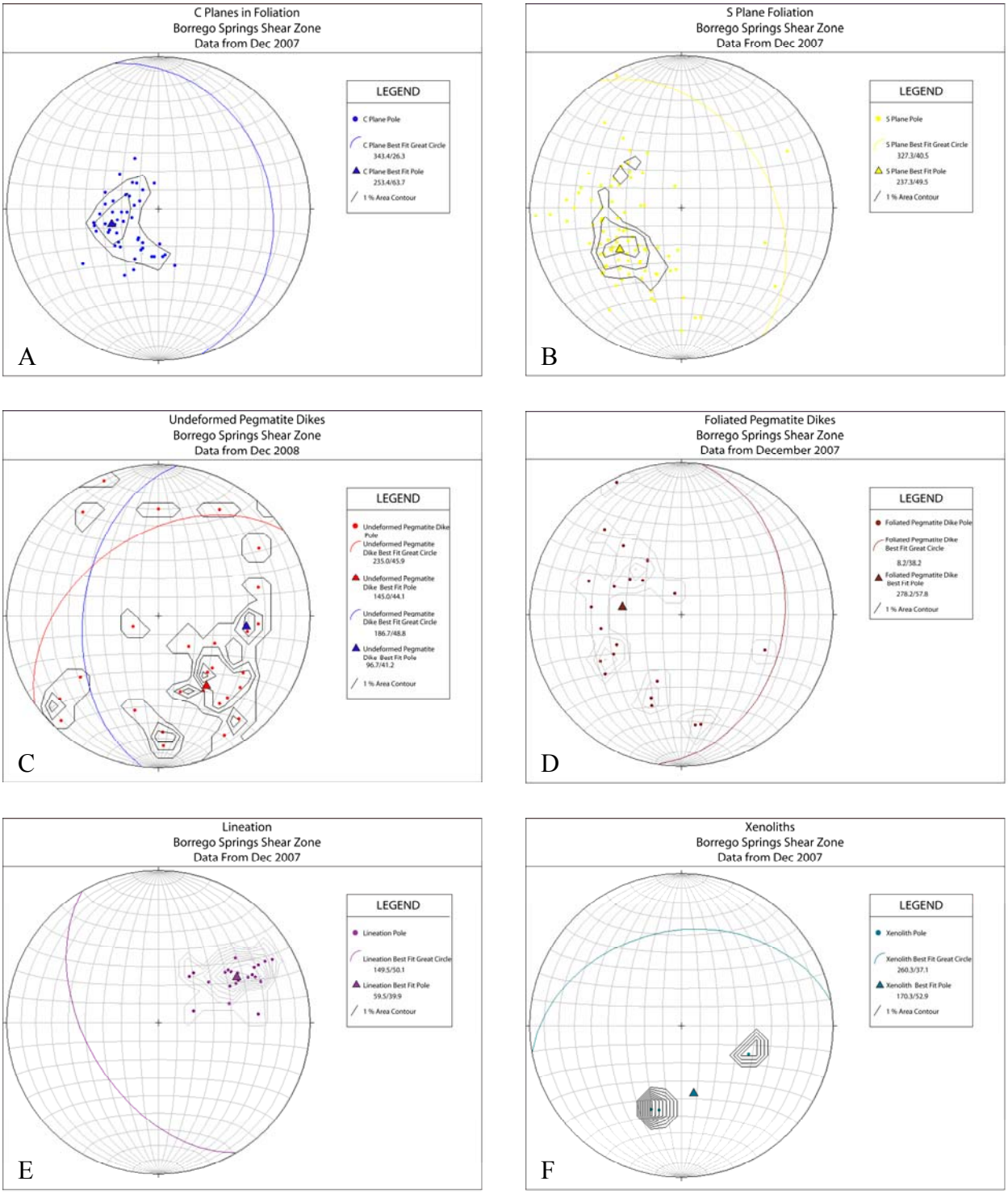

Figure 9A-F: Stereonet diagrams of data from Dec 2007. A: C-Planes, B: S-Planes, C: Undeformed pegmatite dikes, D: Foliated pegmatite dikes, E: Mylonitic Lineation, F: Xenoliths. All diagrams show best fit great circle as statistical average and best fit poles.

Both the class data and data collected in Dec 2007 were compiled and analyzed in a similar fashion. The composite averages of all this data was only slightly different (Figure 10). Average orientations of S and C were 1.3/45.3 and 0.8/24.8 respectively. Lineation of mylonitic tonalite displays an easterly trend: 158.7/51.8 (Figure 10A). The compilation of undeformed pegmatite dikes led to the formation of five general orientations of 233.3/52.8, 207.8/63.7, 45.9/61.6, 353.2/33.1, and 178.9/51.3 (Figure 10B). Foliated pegmatite dikes average at: 2.5/38.0 (Figure 10C).

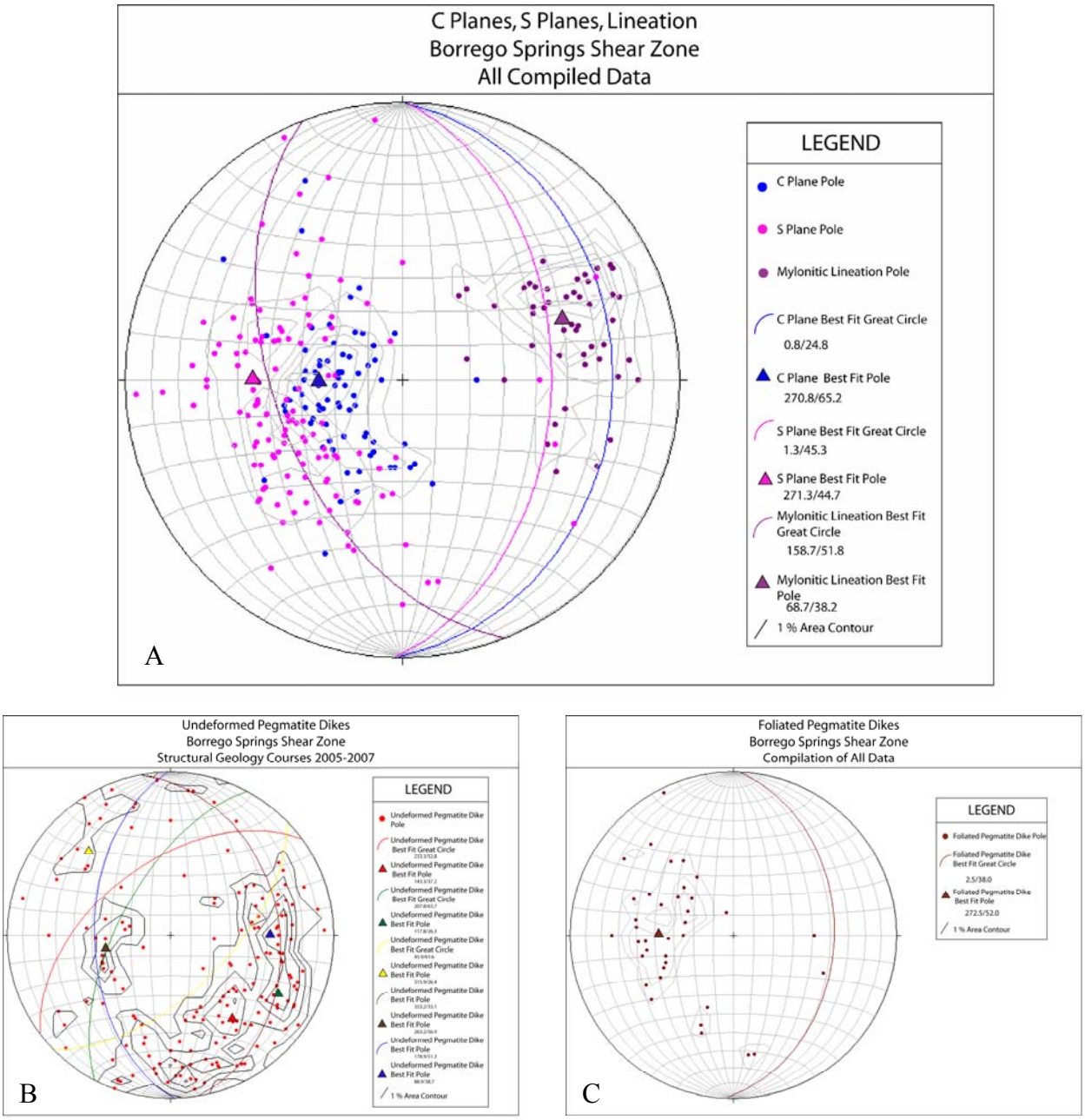

Figure 10A-C: Stereonet of combined data; A: S and C Planes, mylonitic lineation, B: Undeformed Pegmatite Dikes, C: Foliated pegmatite dikes. All diagrams show best fit great circle as statistical average and best fit poles.

Observations on Block Samples

While in the field, oriented hand samples were collected to be used in the laboratory for additional analysis and thin section preparation. These rocks were cut perpendicular to foliation and parallel to lineation. Both fresh faces were lacquered and used in additional macroscopic analysis of the S-C angle. In this instance, the C plane was estimated through the sample and the angle of the S plane was measured with respect to the average C plane (Figure 11).

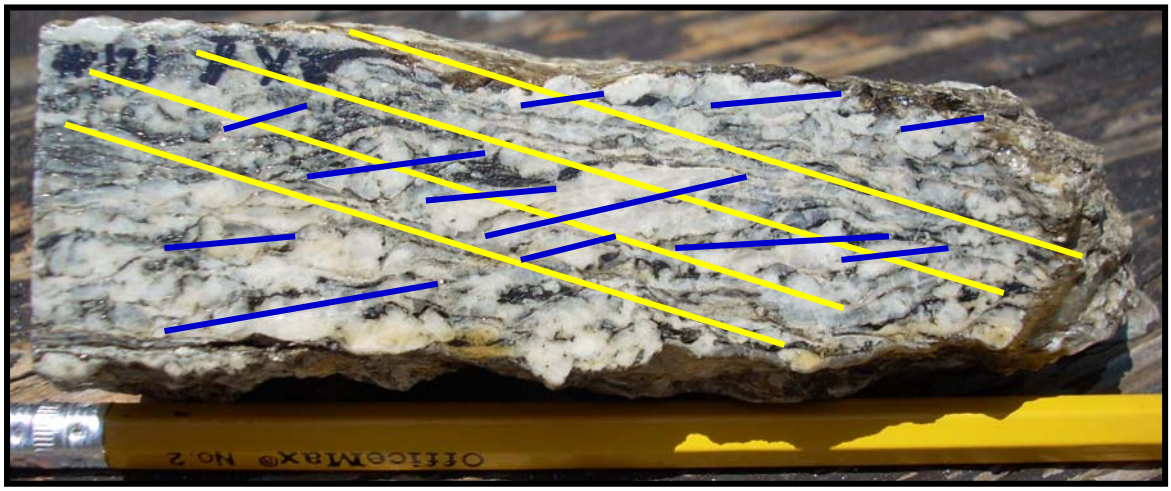

Figure 11: Sample KK121 showing C planes estimated in yellow and S planes in blue measured with respect to the C plane.

This procedure was carried out on seven samples, KK89, KK92, KK102, KK 107, KK 115, KK 121, and KK 158. The calculated averages S-C angle (θ), and shear strain (γ) values are summarized in the following table:

Sample	θ (deg)	γ = (2/tan2θ)
KK89	18.20	2.71
KK92	35.53	0.69
KK102	26.60	1.50
KK107	19.07	2.55
KK115	26.53	1.50
KK121	21.40	2.16
KK158	27.73	1.38

Table 1: θ measured from oriented hand samples at the macroscopic level.

I used the results of the S-C angle analysis to calculate γ values for each of the respective samples using the equation $\gamma = (2/\tan 2\theta)$. Each of these samples were plotted on a graph relating θ to γ (Figure 12). These samples plotted between $\sim 18 < \theta < 36$ degrees and $\sim .5 < \gamma < 3$. Also plotted on this diagram are S-C angles and shear strain values deduced from macroscopic measurements at the same point in outcrop.

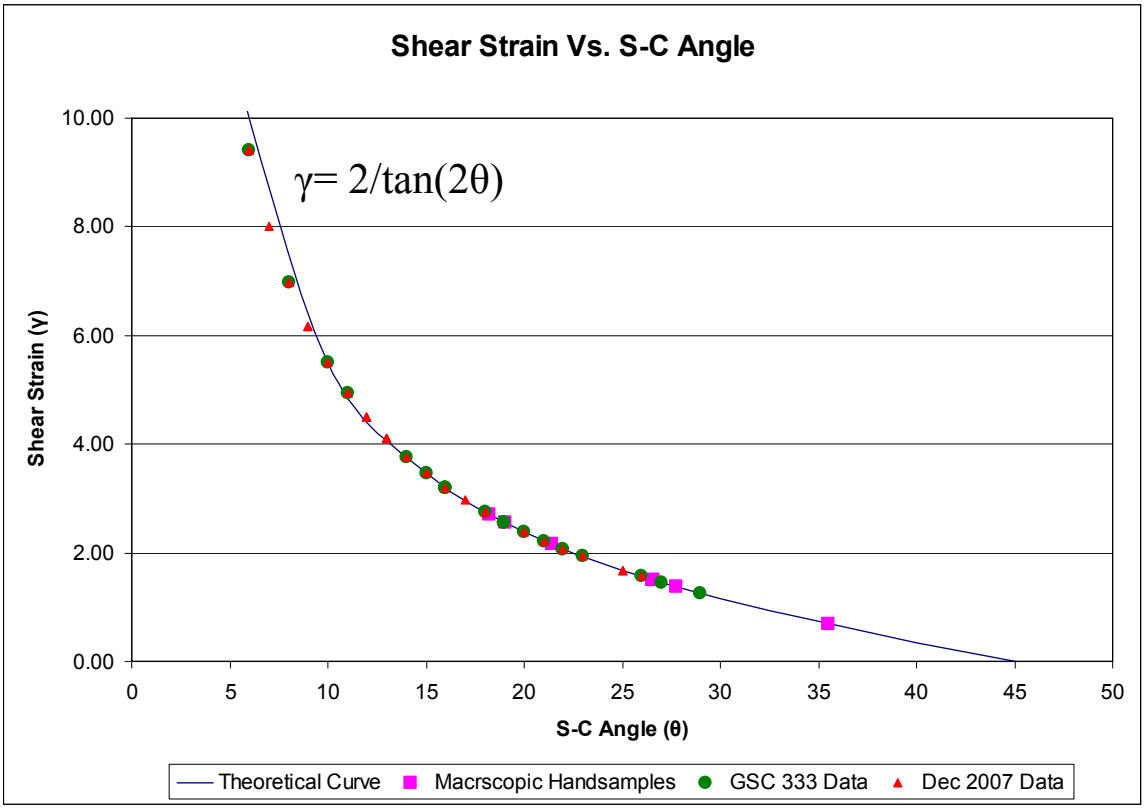

Figure 12: Graph show where all hand sample plot on the theoretical simple shear curve.

Microscopic Observations

Petrographic analysis was preformed on 12 of the 23 oriented hand samples. Of the 12 cut thin sections, the eight cut perpendicular to foliation (XZ direction) were KK89, KK92.2, KK102.2, KK115.1, KK116.1, KK121, KK158.1, and KK 203. Of these, 4 have pairs that were also cut in the direction parallel to lineation (YZ direction). The samples include KK92.1, KK102.1, KK115.2 and KK158.2. The average θ values and standard deviations calculation of the measurements are summarized in Table 2:

	Splanes		Cplanes	Splanes		Cplanes	Splanes		Cplanes	Splanes		Cplanes
Sample	KK89	Grain	KK89	KK92.2	Grain	KK92.2	KK102.2	Grain	KK102.2	KK115.1	Grain	KK115.1
AVG	340		326	368		327	358		342	351		321
DIFF (θ)		14			41			16			30	
STDEVσ	6.97		10.46	14.69		10.29	13.89		11.11	9.22		13.66
		12.57			17.93			17.79			16.49	
Diff Err		14 ± 12.57			41 ± 17.93			16 ± 17.79			30 ± 16.49	

	Splanes		Cplanes	Splanes		Cplanes	Splanes		Cplanes	Splanes		Cplanes
Sample	KK116.1	Grain	KK116.1	KK121	Grain	KK121	KK158.1	Grain	KK158.1	KK203	Grain	KK203
AVG	350		331	375		350	379		402	369		364
DIFF (θ)		19			25			23			5	
STDEVσ	8.09		8.68	6.00		13.29	14.77		11.51	8.50		8.49
		11.86			14.58			18.73			12.01	
Diff Err		19 ± 11.86			25 ± 14.58		23 ± 18.73				5 ± 12.01	

Table 2: The average of all microscopic measurements in the S and C direction, the difference between them (θ), the standard deviation of the measurements. Highlighted samples are used in subsequent analysis.

Further petrographic analysis included the measurement of aspect ratios (Rxz and Ryz) of individual grains (Refer back to Figure 4). Samples used for this analysis include the XZ sections; KK92.2, KK102.2, KK 115.1 and KK 158.1 and YZ sections; KK 92.1, KK102.1, KK 115.2, and KK158.2. These thin sections were viewed and the length of the X, Y and Z dimensions were measured for various feldspars, plagioclase feldspar, quartz, biotite, and hornblende. These data were then used to calculate the aspect ratios of the individual sample using equations (1) through (12) from the methods portion of this paper.

Because the Rxz and Ryz values come from the average of measurements, it is important to note that the arithmetic mean assumes that all grains are initially spherical while the harmonic mean accounts for a non-spherical original shape. Originally elongate minerals will produce greater strained aspect ratios; the harmonic mean reduces this value. While the harmonic mean may seem like the most representative average due to the fact that feldspars and amphiboles are elongate in crystalline form, quartz grains in igneous rocks may have been more spherical originally and therefore, their strained shape may be better represented by the arithmetic mean. Considering these two issues, both the

harmonic and arithmetic averages were calculated and all subsequent 3-D strain calculations were carried out with respect to both. The results of these calculations are summarized in Table 3:

	Sample	Normalized KK92	Normalized KK102	Normalized KK115	Normalized KK158
Harmonic	Aspect Ratio; X:Y:Z	4.25:4.12:1.0	4.15:3.91:1.0	5.05:3.64:1.0	4.80:2.72:1.0
Arithmetic	Aspect Ratio; X:Y:Z	4.70:4.43:1.0	4.54:4.08:1.0	5.53:4.25:1.0	5.14:2.93:1.0
Harmonic	Semi-Axis a	2.13	2.08	2.53	2.40
	Semi-Axis b	2.06	1.96	1.82	1.36
	Semi-Axis c	0.50	0.50	0.50	0.50
Harmonic	Radius r	1.30	1.27	1.32	1.18
Arithmetic	Semi-Axis a	2.35	2.26	2.77	2.57
	Semi-Axis b	2.22	2.04	2.13	1.47
	Semi-Axis c	0.50	0.50	0.50	0.50
Arithmetic	Radius r	1.38	1.32	1.43	1.23
Harmonic	Longitudinal Strain e_x	0.64	0.64	0.92	1.04
Arithmetic	Longitudinal Strain e_x	0.71	0.71	0.93	1.08
Harmonic	Longitudinal Strain e_y	0.59	0.54	0.38	0.16
Arithmetic	Longitudinal Strain e_y	0.61	0.54	0.48	0.19
Harmonic	Longitudinal Strain e_z	-0.61	-0.61	-0.62	-0.58
Arithmetic	Longitudinal Strain e_z	-0.64	-0.62	-0.65	-0.60
Harmonic	Principle Stretch Sx	1.64	1.64	1.92	2.04
Arithmetic	Principle Stretch Sx	1.71	1.71	1.93	2.08
Harmonic	Principle Stretch Sy	1.59	1.54	1.38	1.16
Arithmetic	Principle Stretch Sy	1.61	1.54	1.48	1.19
Harmonic	Principle Stretch Sz	0.39	0.39	0.38	0.42
Arithmetic	Principle Stretch Sz	0.36	0.38	0.35	0.40
Harmonic	Rxz = Sx/Sz	4.50	4.33	5.49	5.03
Arithmetic	Rxz = Sx/Sz	4.70±1.64	4.52±1.15	5.53±1.09	5.14±1.12
Harmonic	Rxy = Sx/Sy	1.03	1.06	1.39	1.76
Arithmetic	Rxy = Sx/Sy	1.06	1.11	1.30	1.75
Harmonic	Ryz = Sy/Sz	4.12	3.91	3.63	2.72
Arithmetic	Ryz = Sy/Sz	4.43	4.08	4.25	2.93

Table 3: Summary of properties determined from aspect ratios of the strain ellipsoid.

These aspect ratios were used to calculate principle stretches Sx, Sy, and Sz values which were then plotted on a Flynn diagram to determine if the shear zone had undergone constriction, flattening, or simple shear. According to the Flynn Diagram (Figure 13), these four samples plot within the flattening field.

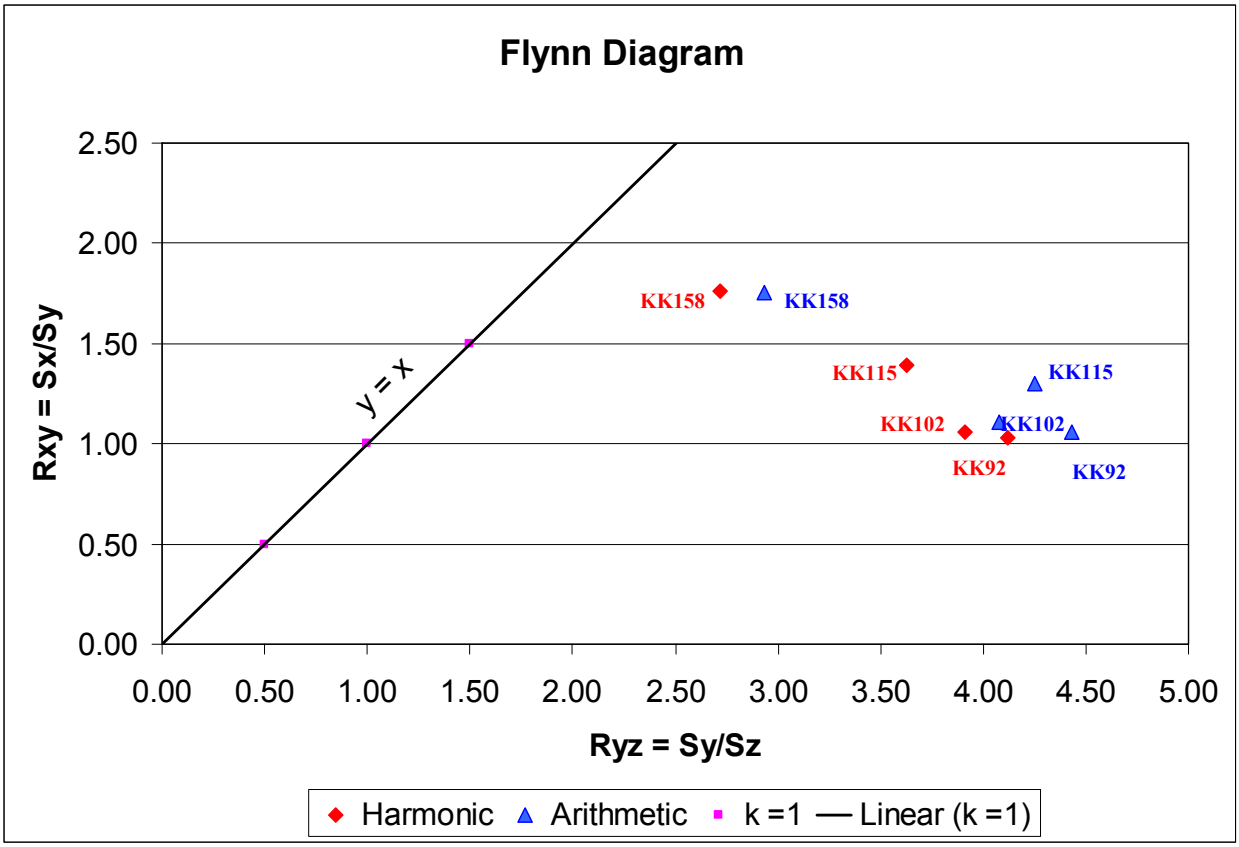

Figure 13: Flynn Diagram showing where each of the samples plot in relation to the y=x simple shear line. The X-axis represents the pure flattening strain and the Y-axis represents pure constriction strain.

To compare the results of the actual strain ellipsoid as defined Rxz, Rxy, and Ryz, to the simple shear model, graphs were plotted with each of these individual samples against the calculated theoretical simple shear, S-C model. These data were plotted on a variety of graphs including θ vs. Rxz (Figure 14) and γ vs. Rxz (Figure 15). These graphs show that the samples plot both above and below the predicted simple shear model, and do not follow the same style of curve. However, there is some overlap of error bars onto the simple shear curve.

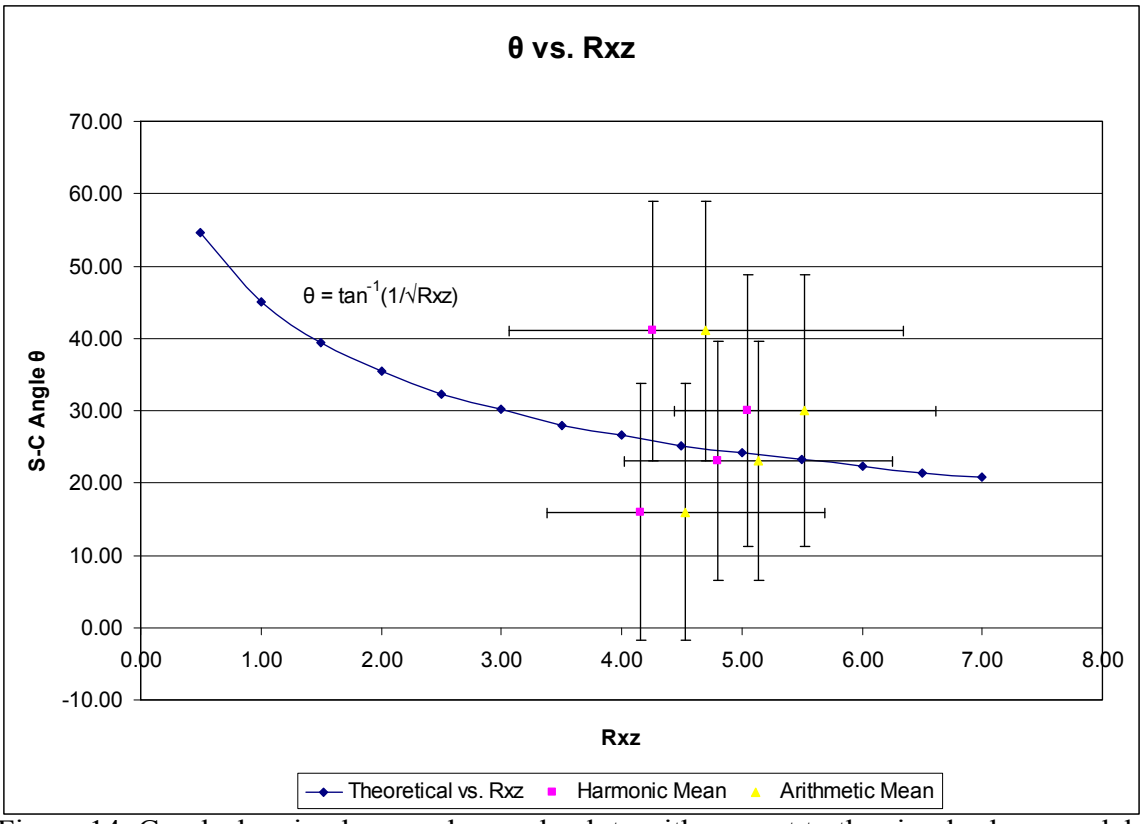

Figure 14: Graph showing how each sample plots with respect to the simple shear model.

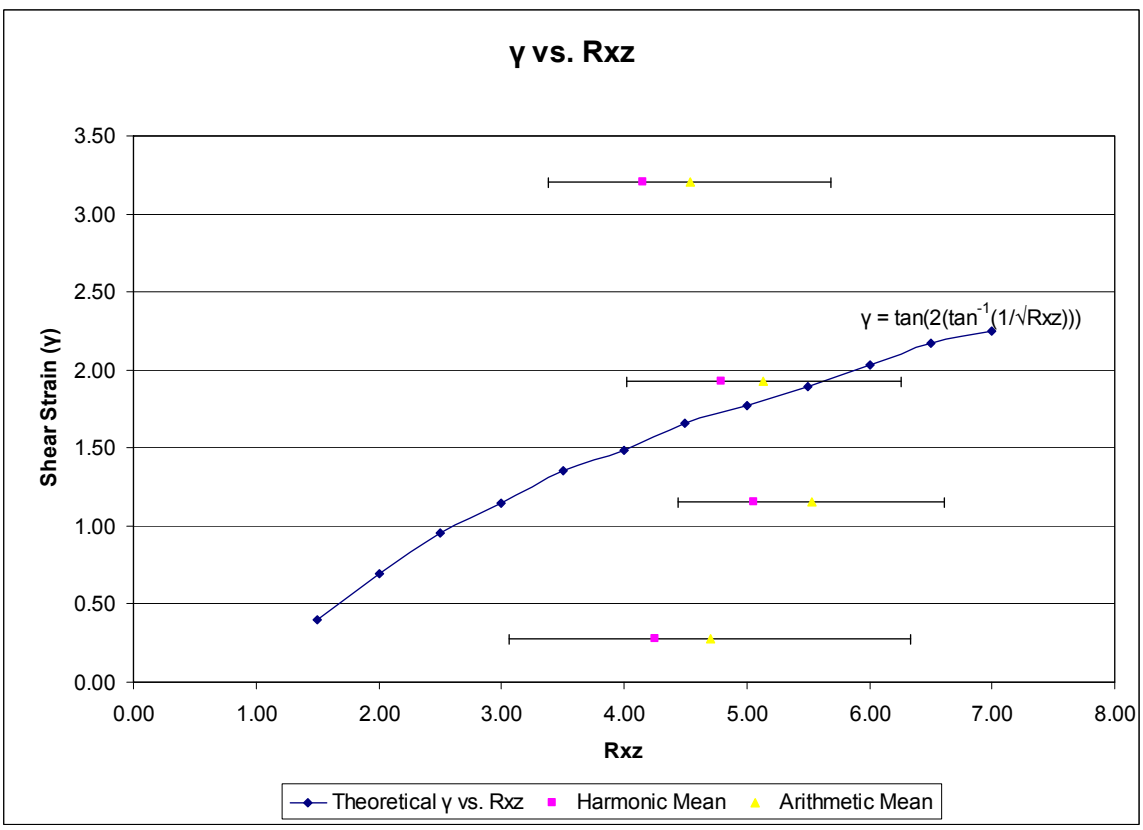

Figure 15: Graph showing how each sample plots with respect to the simple shear model.

Also included in my analysis are various histograms describing the relationship between the S-C angle of each sample to a given mineral (feldspar, plagioclase feldspar, quartz, biotite, and hornblende) in each sample. In theory, the lower the S-C angle, the higher the amount of shear strain. Under these metamorphic conditions, it is expected that the quartz grains will have deformed more than the other more rigid and blocky feldspars. The histogram in Figure 16 shows this feature in the majority of the samples.

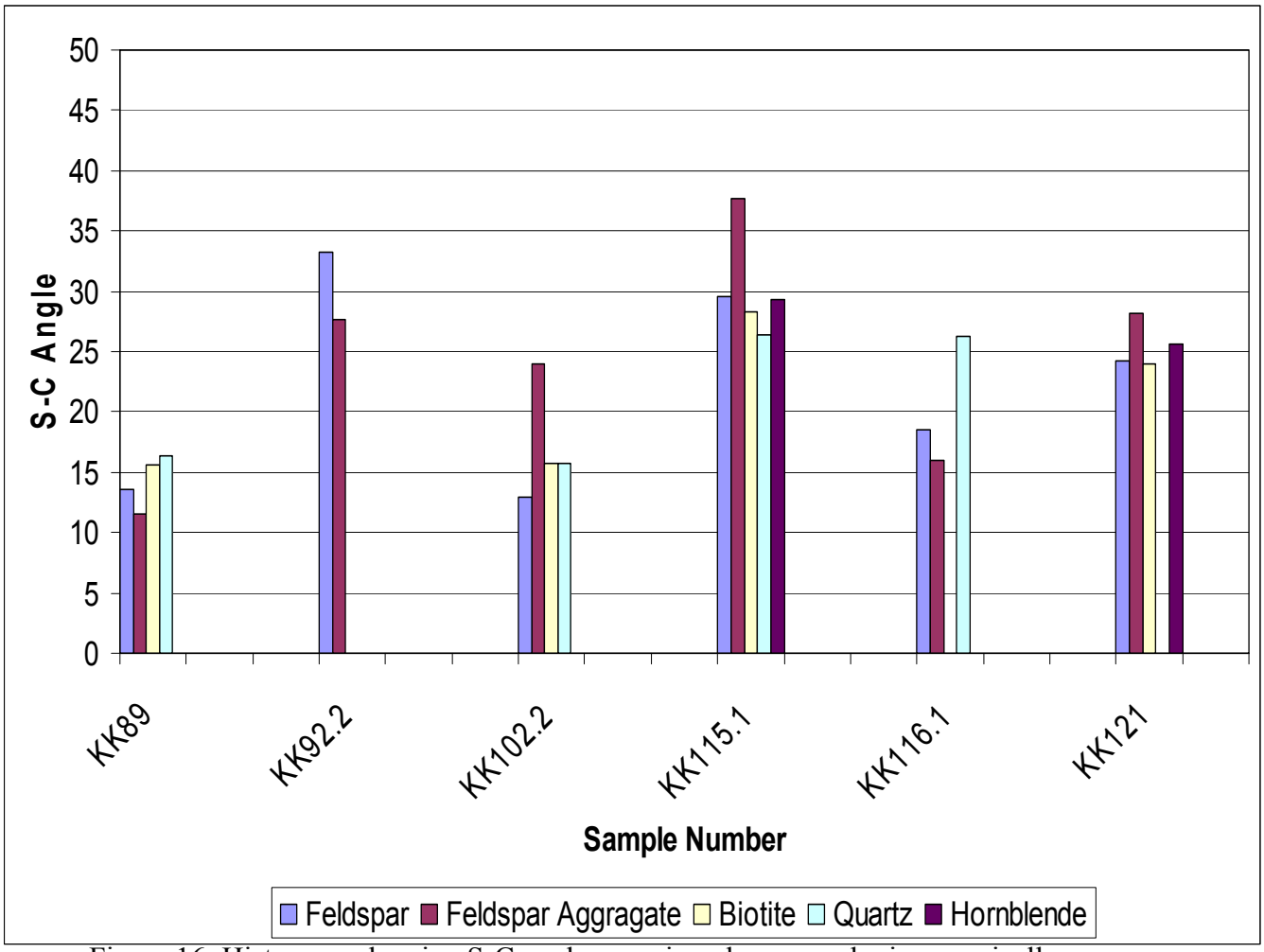

Figure 16: Histogram showing S-C angle per mineral measured microscopically per sample.

An additional set of histograms relates the harmonic Rxz and Ryz and Arithmetic Rxz and Ryz values per sample to each individual mineral in that sample. Similar to the S-C angle per mineral analysis, quartz is expected to react most easily to these conditions. This characteristic is noted in all the samples shown in Figure 17A-B.

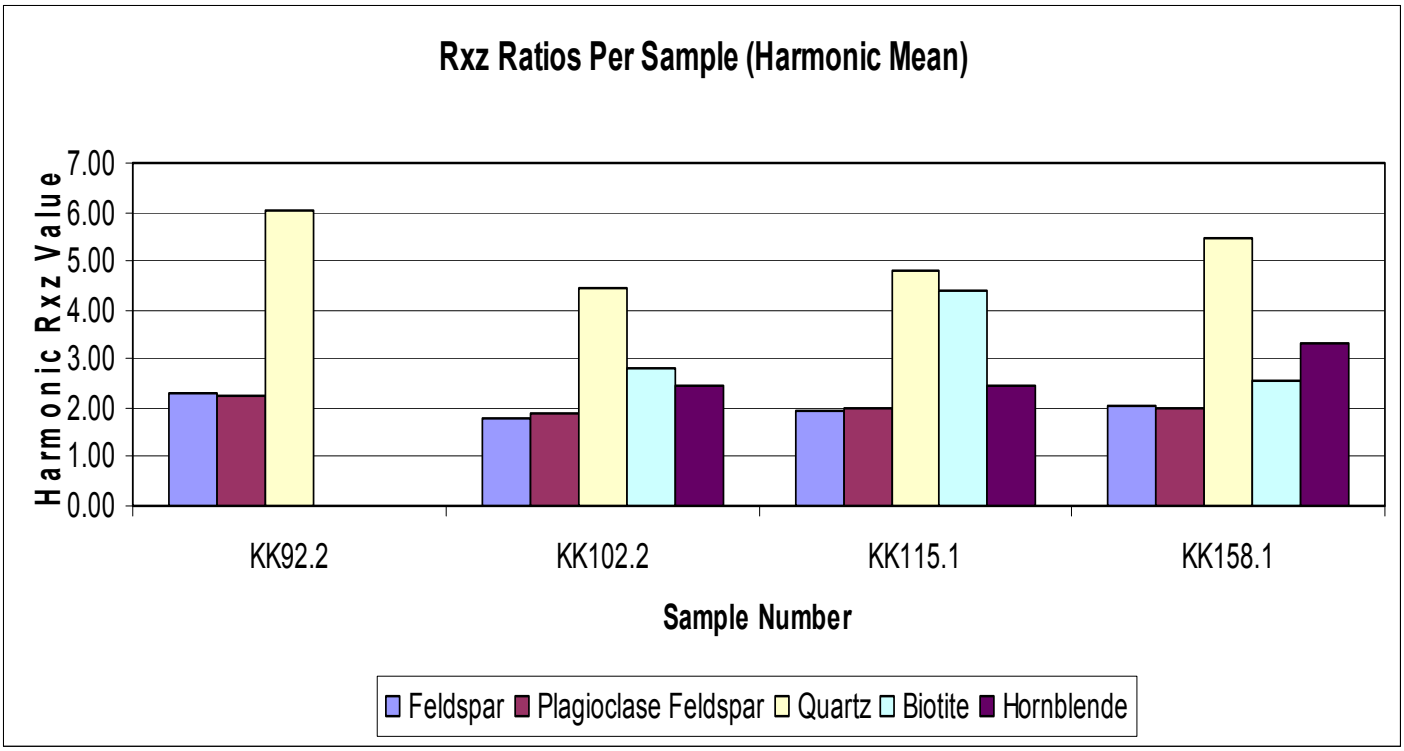

Figure 17A: Histogram showing the variable aspect ratios per mineral in four samples.

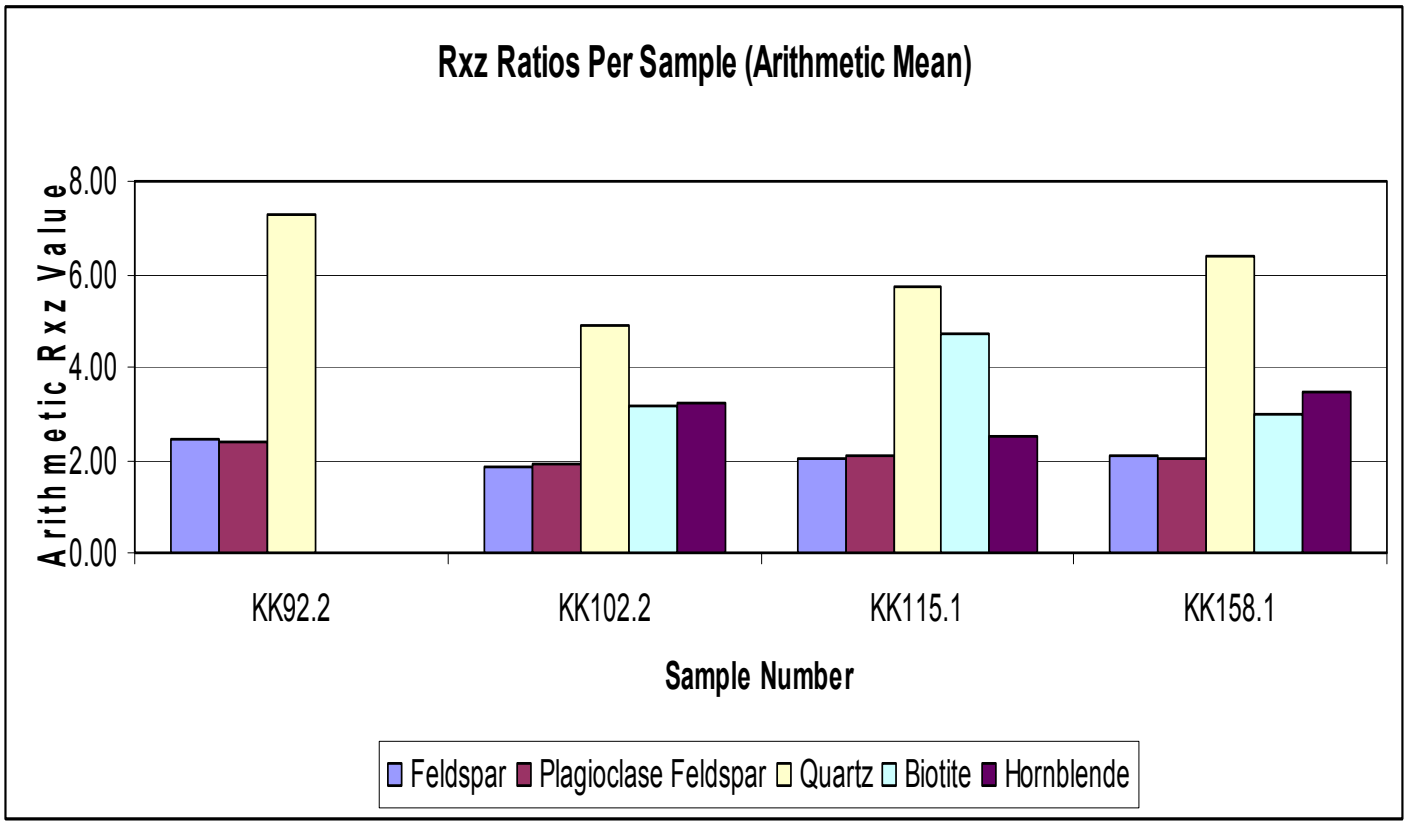

Figure 17B: Histogram showing the variable aspect ratios per mineral in four samples.

DISCUSSION AND INTERPRETATION

Macroscopic Analysis

There are many types of shear zones. Preliminary inspection suggested that the Borrego Springs Shear Zone (BSSZ) was deformed by non-coaxial simple shear/plane strain. This type of deformation occurs when one dimension of grains in a rock remains fixed and other dimensions rotate relative to it. In an idealized situation, highest amounts of strain will occur in the middle of the shear zone, shear planes (C-Planes) will develop parallel to the boundaries of the shear zone, and S-Plane foliation will occur at some angle to the C-Planes. This S-C angle (θ) will decrease as the shear zone is subjected to increased amounts of strain (Figure 1). If simple shear is known to prevail, simplified two-dimensional equations can be utilized to constrain the dimensions of the strain ellipsoid which constrains values of shear strain (γ). These equations include the following:

$$Rxz = Sx^2 \qquad \text{(Eq: 13)}$$

$$Rxz = (1/Sz)^2 \qquad \text{(Eq: 14)}$$

$$(Sx)(Sz) = 1.0 \qquad \text{(Eq: 15)}$$

This concept has been used in my investigation as a model by which to test the hypothesis stated in the Introduction of this paper and as a reference for discerning the nature of deformation through the BSSZ.

Previous investigation and field observations both denote a top-to-the-west sense of shear through the BSSZ (Simpson and GSC 333 Classes). The sheared plutonic section of the BSSZ overlain by a belt of sheared metasedimentary rock. The orientation of the upper shear zone boundary would occur to the east, but is not exposed. To the west, a "mylonitic front" marks the transition from mylonitic tonalite into the undeformed tonalite. It can be considered the approximate base of the shear zone (or the lower shear zone boundary).

In the ideal case, S foliation planes tend to bend in the direction of shear in an effort to orient themselves parallel to the boundaries of the shear zone. This is denoted by the variation in dip of the S Planes on this map. Once analyzed, these data began to show

that high strain bands occur throughout the BSSZ where S-planes have shallower east dips close to the dips of the C-planes. This can be seen in the field by interspersed lenses of ultramylonites within a weakly foliated tonalite. This is demonstrated on the topographic in Figure 18. This image was created by interpolating the data in Table 1 by nearest neighbor using GIS software. These relationships clearly show that shear strain in the BSSZ is heterogeneous. Thus displacement through the shear zone is also heterogeneous with increased amounts of displacements occurring along the ultramylonites lenses and smaller amounts occurring else where. A representation of this effect is found in sample KK203. This sample has a $\theta = 5^{o}$ and $\gamma = 11.34$. It can also be concluded that these ultramylonite lenses contain C-Planes that are aligned approximately parallel to the shear zone boundary.

Macroscopic data was also used in the production of stereo net diagrams. These diagrams are useful in the determination of best fit averages of all field measurements the data. These diagrams clearly illustrate five distinctive orientations of undeformed pegmatite dikes west of the shear zone (Refer back to Fig 10B). Into the shear zone, these dikes begin to deform and rotate into the direction of foliation as denoted on an additional stereonet (Refer back to Fig 10C).

A rotation pattern can also be seen in Google Earth satellite photos. These photos have been overlain on a topographic map of the area and the dikes have been outlined for obvious inspection. Applying the "rule of V's" for the outcrop pattern, it is easy to see the rotation of the dikes into the E-dipping shear zone. (Refer to Fig 19 below). Also strikes of the dikes display a transition from ~trimodal trends in Culp Valley to uniformly north striking through Montezuma Grade.

The stereonet plots demonstrate the average lineation in the BSSZ is directed predominantly east/southeast (Refer back to Fig 10a). Likewise, the diagrams of S and C planes depict the general trends through the BSSZ. It becomes clear that the strikes of S and C planes are approximately parallel and show a characteristic difference in dip. This difference in S and C plane dip is used to macroscopically determine θ and γ. The average orientation of S and C planes are 1.3/45.3 and 0.8/24.8 respectively. The figures correspond to $\theta = 20.5^{o}$ and a $\gamma = 1.68$. These values are a representative gross average for the outcrops studied.

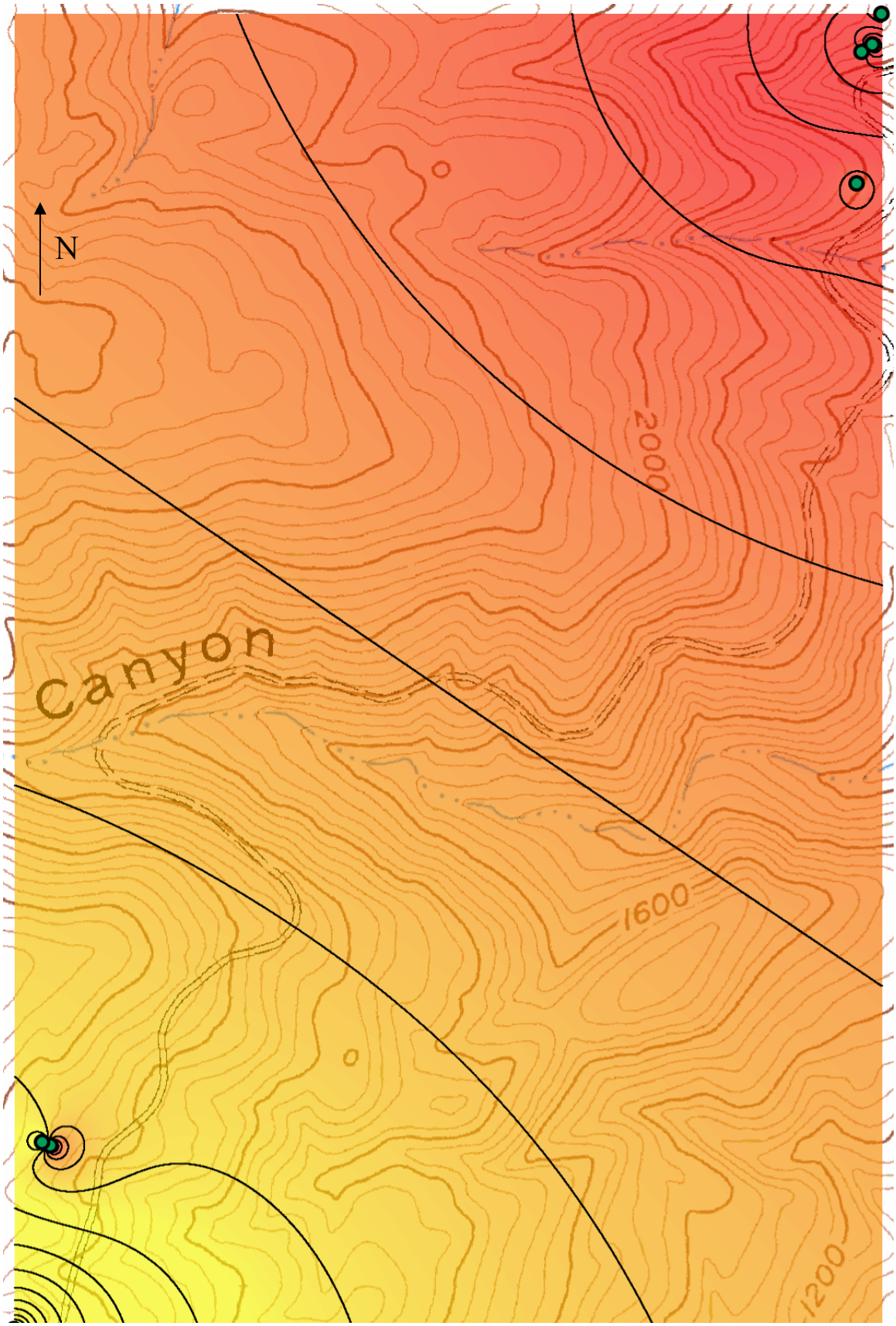

Figure 18: IDW interpolation and $\gamma = 0.05$ contour intervals based on data from Table 1. Color gradient from yellow $\gamma = 1.55$ to red $\gamma = 2.20$

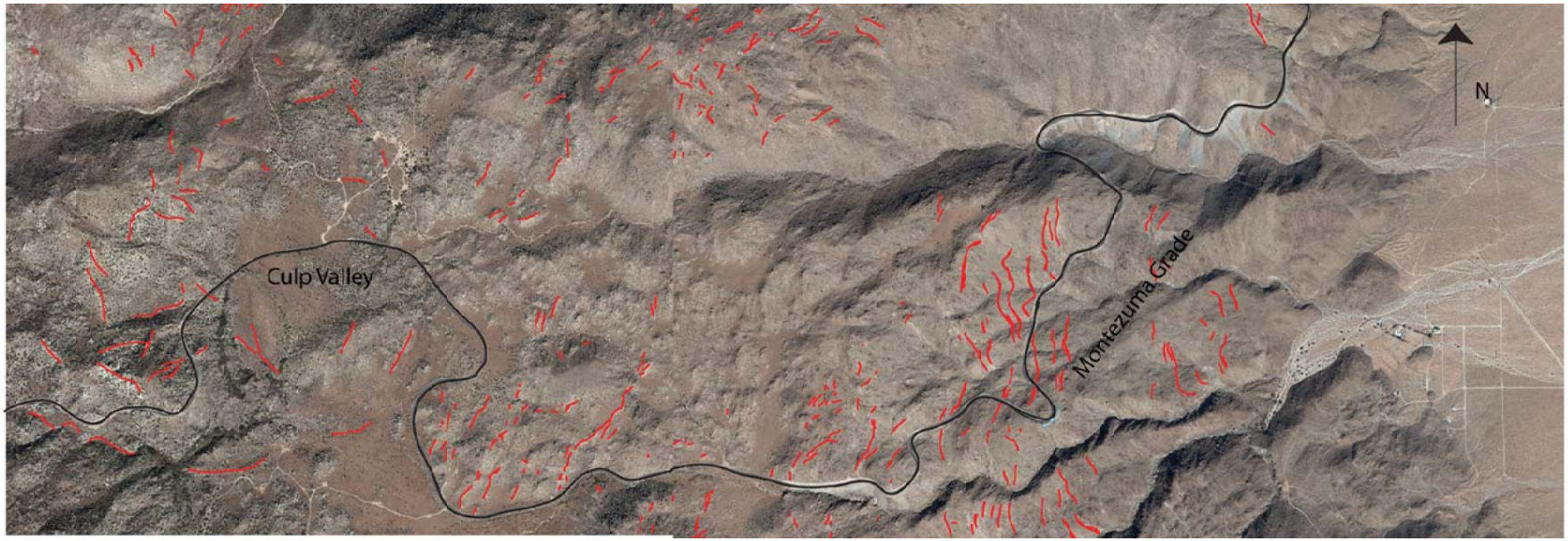

Figure 19: Google Earth satellite image of the study area. Black line outlines the highway S22 Red lines outline undeformed pegmatite dikes near Culp Valley, west of the shear zone and foliated pegmatite dikes through Montezuma grade in the BSSZ

Using averages it is possible to approximate displacement across the BSSZ. The application of the equation $D=\int_0^x \gamma dx$; where x is the thickness of the shear zone. It is determined that there was an average of ~4.64km of displacement assuming the thickness of the BSSZ is ~2.76km. However, we have already proven that strain through the BSSZ is heterogeneous; therefore this γ value represents only an average and may be overestimated in areas of low shear and underestimated in ultramylonite zones. We believe that the majority of slip occurred in these ultramylonite zones and therefore may relate to a larger amount of displacement.

Microscopic Analysis

Twelve thin sections were cut from orientated hand samples collected in the field. These thin sections were used in microscopic analysis of S-C angle and in the measurement of the X, Y, and Z dimensions of grains in order to calculate the strain ellipsoid. The results of this study are outlined in the Data and Results section. Here we will discuss these results and offer an interpretation.

Various graphs and histograms were created to statistically analyze all the data. Additionally, these methods facilitate our ability to discern the nature of deformation. Firstly, the Flynn diagram was created which determines which of three environments rocks were deformed; 1) constriction, 2) simple shear, or 3) flattening strain. As shown in the previous section, the four samples all plotted in the flattening strain portion of the diagram. This can be explained by the overburden of material on top of the deformation zone. The weight of this block causes the minerals in our samples to be squashed in both the X and Y directions.

Secondly, graphs of θ vs. Rxz (Fig. 13) and γ vs. Rxz (Fig. 14) were created to compare the results of the strain ellipsoid to the simple shear model. While it is not immediately obvious that these samples follow the same curve as the simple shear model, they all fit the model within the error bounds of this investigation. Standard deviation was found for all the measurements of S and C planes and the two were combined in the error equation:

$$\sigma_\theta = \sqrt{((\text{Stdev S})^2 + (\text{Stdev C})^2)} \qquad \text{(Eq: 16)}$$

The values found from this equation were used to supply to Y error bars in the θ vs. Rxz graph. Standard deviation of measurements used to find the arithmetic Rxz were used to provide the X error bars in this graph. These values are summarized in Table 4:

Sample	Normalized KK102.2	Normalized KK92.2	Normalized KK158.1	Normalized KK115.1
Normalized Harmonic Mean Rxz	4.15	4.25	4.80	5.05
Normalized Arithmetic Mean Rxz	4.54	4.70	5.14	5.53
S-C Angle (θ)	16.00	41.00	23.00	30.00
Shear Strain (γ)	3.20	0.28	1.93	1.15
Standard Deviation Error (σ_θ)	17.79	17.93	16.49	18.73
f'(θ)	-14.24	-4.08	-7.73	-5.33
$\sigma_\gamma = \sigma_\theta * f'(\theta)$	-253.41	-73.14	-127.47	-99.89
Standard Deviation Arithmetic Rxz	1.15	1.64	1.12	1.09

Table 4: Summarizes the sample according to Rxz value, θ and γ. This table also includes the error values used in each of the graphs.

The graph of γ vs. Rxz (Fig. 14) is more erratic. Only one of samples of the curve fit the simple shear model within the error boundaries of Rxz. As shown in the table above, the error with respect to γ was calculated according to the following steps for error analysis of a function of θ:

Error of γ

1) Take derivative of $\gamma = 2/\tan 2\theta = f(\theta)$

1a) $f'(\theta) = -4*(1/\sin^2(2\theta))$

2) Plug θ values into f'(θ)

3) Multiply value from part 2 by the standard deviation of theta (σθ) to get σγ

The results of this analysis are summarized in Table 4. The values of σγ are very high. Error analysis reveals that there is a great deal of local scattering in the measurements. This can be attributed to the varied orientation of S and C planes on the microscopic scale of <4mm. At this scale it may be that C plans are either bent or skewed by large blocky

feldspar grains. Although there is a substantial variation in these measurements, the average of numerous measurements may provide the best θ and γ values.

In order to quantify and visualize how varied amounts of strain affect specific minerals under these metamorphic conditions, histograms were created that show how the aspect ratio (Rxz) of each mineral changes per sample (Refer back to Figure 17A-B). These diagrams support the general definition of mineral deformation at the temperatures and pressures associated with upper greenschist / lower amphibolite facies metamorphism. Quartz grains are shown to have the highest Rxz values in each sample, while the mafics (hornblende and biotite) deform more than various feldspars which tend to remain blocky and even undergo antithetic slip. The last histogram (Figure 17B) explains the relationship between S-C angle per mineral in each sample. The relationship between θ and γ through the equation $\gamma = 2/\tan(2\theta)$ explains that as θ decreases, γ increases. As mentioned before, the quartz grains are the most deformed under these conditions, therefore it is expected that the S-C angle of the quartz grains would be the smallest. According to the histogram, this is not always the case. This theory holds true in only two of the four samples where quartz data is available. In two others, the opposite effect is true. It is possible that larger, blocky feldspar grains interfered with deformation patterns of other minerals. Additionally, it may be suggested that local variations in fluid conditions, metamorphic grade (temperature especially), or strain rate may have led to heterogeneous mineral deformation.

CONCLUSIONS

From this investigation I conclude the following: 1) Shear strain through the BSSZ is heterogeneously distributed 2) A map has been created identifying the high and low strain areas of the shear zone. With the aid of this map, additional samples can be collected and supplementary analysis conducted to further constrain the characteristics of the BSSZ.

3) Mineralogic analysis shows that mineral behavior in response to shearing deformation is also heterogeneous. 4) Grain shapes at varying levels of strain do not convincingly fit the simple shear model. Instead, the BSSZ has been affected by a significant flattening component shear. 5) Analysis at different scales produce varying

results; at this point it is uncertain which scale of observation provides the most accurate shear strain values. 6) In response to the questions and hypothesis stated in the Introduction portion of this paper, I conclude that there is a simple shear component that acted upon the BSSZ, however other deformation effects are observed. Therefore, more analysis is required in order to determine the extent of the effects of simple shearing.

APPENDIX A: *THIN SECTION S-C PLANE RAW DATA*

Table of raw data collected from thin section samples; KK89, KK92.2, KK102.2, KK115.1, KK 116.1, KK121, KK158.1, and KK203. These sections were cut perpendicular to foliation. Values are angles measured on a Leitz Petrographic microscope using a station stand. All numbers were measured with north being at 0 or 360º. Measured grains were identified with the following key: FF = Feldspar aggregate, F = Feldspar, Q = Quartz, B = Biotite, H = Hornblende. Data used for θ and γ calculations:

	Splanes		Cplanes	Splanes		Cplanes	Splanes		Cplanes	Splanes		Cplanes
Sample	KK89	Grain	KK89	KK92.2	Grain	KK92.2	KK102.2	Grain	KK102.2	KK115.1	Grain	KK115.1
	327	F	342	355	F	321	325	B	342	355	F	323
	349	B	345	352	F	319	352	Q	335	367	F	317
	342	Q	335	379	F	326	346	B	343	345	H	325
	348	Q	330	358	F	328	345	B	346	352	F	313
	337	F	336	380	F	327	338	B	367	360	H	335
	336	FF	335	378	F	323	340	F	345	353	Q	297
	331	FF	335	321	FF	327	348	H	361	363	F	335
	338	F	345	376	F	316	342	F	347	349	F	314
	343	B	340	377	F	343	344	F	350	360	FF	312
	343	B	327	382	F	324	365	FF	346	343	H	328
	342	Q	338	357	F	319	369	B	357	380	FF	326
	333	FF	309	374	F	347	335	Q	351	352	FF	327
	340	Q	320	360	FF	317	379	B	349	348	H	331
	334	F	310	383	FF	328	357	F	334	345	FF	340
	352	Q	319	380	F	343	365	FF	334	345	Q	323
	335	FF	312	383	F	314	369	FF	321	344	B	337
	320	F	322	354	F	328	372	B	346	355	FF	329
	346	FF	322	375	F	324	362	F	330	350	F	290
	344	F	324	370	F	328	363	F	337	352	FQ	293
	343	Q	325	352	F	344	362	F	341	350	F	314
	343	FF	319	360	F	328	371	B	349	344	B	303
	338	B	335	375	F	321	375	B	337	357	B	323
	341	B	333	376	F	324	364	F	349	355	F	311
	330	Q	310	373	F	344	357	F	345	347	F	313
	352	F	345			315	371	Q	339	352	F	319
	348	F	333			346	358	F	354	342	F	317
	349	FF	337			316	373	Q	365	335	F	334
	349	B	334				365	FF	336	348	H	354
	343	F	348						336	335	H	333
	348	F	335						344	338	F	337

	335	F	315						337	360	H	305
	346	F	315						337	354	FF	317
	333	FF	324						347	366	H	312
	338	B	312						336	357	F	313
	335	F	322						315	345	F	310
	349	F	322						329	344	F	307
	334	B	327						337	347	FQ	330
	338	F	340						334	335	FQ	340
	331	F	330						320	347	F	320
	340	B	325						350	345	F	328
	340	F	326									
	352	F	315									
	334	FF	320									
	338	F	312									
	337	F	317									
	341	B	330									
	335	FF	326									
	340	F	308									
			327									
			330									
			314									
			328									
			331									
			328									
			325									
			311									
			340									
			333									
			314									
			318									
				18								
AVG	**340**		**326**	**368**		**327**	**358**		**342**	**351**		**321**
DIFF (θ)		**14**			**41**			**16**			**30**	
STDEV	**6.97**		**10.46**	**14.69**		**10.29**	**13.89**		**11.11**	**9.22**		**13.66**
		12.57			17.93			17.79			16.49	
Diff Err		14 ± 12.57			41 ± 17.93			16 ± 17.79			30 ± 16.49	

	Splanes		**Cplanes**	**Splanes**		**Cplanes**	**Splanes**		**Cplanes**	**Splanes**		**Cplanes**
Sample	**KK116.1**	**Grain**	**KK116.1**	**KK121**	**Grain**	**KK121**	**KK158.1**	**Grain**	**KK158.1**	**KK203**	**Grain**	**KK203**
	353	F	336	371	F	344	385		392	378		352
	345	F	325	372	B	364	370		403	378		360
	340	FF	337	382	F	356	381		410	380		358
	343	FF	328	376	FF	367	375		390	378		362
	347	F	324	370	B	363	325		394	380		359

	356	FF	328	375	FF	349	403		410	376		348
	354	F	336	380	FF	351	373		424	364		358
	360	F	313	377	FF	336	383		400	365		353
	345	F	317	372	F	363	370		399	369		364
	350	F	324	377	F	367	380		389	370		359
	348	QF	330	375	FF	337	380		405	368		364
	350	FF	321	375	FF	345	382		393	369		350
	345	F	333	373	F	367	375		390	371		341
	355	F	333	364	F	363	373		393	367		349
	354	F	332	369	B	362	395		415	376		359
	349	F	338	375	H	333	399		422	376		349
	350	F	337	385	F	337	395		396	373		363
	351	F	333	375	F	337	382		389	371		374
	350	F	331	372	H	347	377		409	364		378
	345	F	345	400	FF	350	380		425	377		366
	350	F	295	380	H	353	375		390	367		379
	345	F	337	375	FF	364	375		400	369		359
	355	F	334	375	F	327	383		401	367		378
	352	Q	331	370	F	329				370		366
	350	FF	333	370	FF	346				383		354
	365	Q	330	380	FB	341				388		367
	368	F	338	372	F	343				377		368
	364	FQ	337	371	B	335				366		357
	345	F	336	373	B	328				375		363
	343	FF	325	370	F	333				376		364
	325	F	338	375	B	333				375		367
			330	372	F	323				358		360
			334	378	Q	344				354		368
			341	370	F	358				357		365
			331	378	F	356				368		365
			338	377	F					356		358
			333	385	B					362		367
			330	377	B					355		363
			335	380	F					362		372
			323							361		386
										355		368
										358		365
										359		365
										358		358
										360		367
												363
												372
												371
												364
												375
												373
												362
												375

												362
												375
												365
												369
												373
												370
												361
												353
												352
												363
				15			19		42	9		
AVG	**350**		**331**	**375**		**350**	**379**		**402**	**369**		**364**
DIFF (θ)		**19**			**25**			**23**			**5**	
STDEV	**8.09**		**8.68**	**6.00**		**13.29**	**14.77**		**11.51**	**8.50**		**8.49**
		11.86			14.58			18.73			12.01	
Diff Err		19 ± 11.86			25 ± 14.58			23 ± 18.73			5 ± 12.01	

APPENDIX B*: SPECIFIC MINERALOGIC ANALYSIS IN THIN SECTION*

The average C plane angle was found from the above table. The difference in S – C angle per mineral is summarized in the following tables. This data was used to construct Figures 16 and 17.

KK92.2	
355	F
352	F
379	F
358	F
380	F
378	F
376	F
377	F
382	F
357	F
374	F
380	F
383	F
354	F
375	F
370	F
352	F
360	F
375	F
376	F
373	F
370	
43	
321	FF
360	FF
383	FF
355	
28	

KK102.2	
340	F
342	F
344	F
357	F
362	F
363	F
362	F
364	F
357	F
358	F
355	
13	
365	FF
365	FF
369	FF
365	FF
366	
24	
325	B
346	B
345	B
338	B
369	B
379	B
372	B

KK115.1	
355	F
367	F
352	F
363	F
349	F
350	F
350	F
355	F
347	F
352	F
342	F
335	F
338	F
357	F
345	F
344	F
347	F
345	F
350	
30	
360	FF
380	FF
352	FF
345	FF
355	FF
354	FF
358	
38	
344	B
344	B
357	B

	KK116.1	
	353	F
	345	F
	347	F
	354	F
	360	F
	345	F
	350	F
	345	F
	355	F
	354	F
	349	F
	350	F
	351	F
	350	F
	345	F
	350	F
	345	F
	355	F
	368	F
	345	F
	325	F
AVG	**350**	
DIFF	**19**	
	340	FF
	343	FF
	356	FF
	350	FF
	350	FF
	343	FF
AVG	**347**	
DIFF	**16**	

KK121	
371	F
382	F
372	F
377	F
373	F
364	F
385	F
375	F
375	F
370	F
372	F
370	F
372	F
370	F
378	F
377	F
380	F
374	
24	
376	FF
375	FF
380	FF
377	FF
375	FF
375	FF
400	FF
375	FF
370	FF
378	
28	
372	B
370	B
369	B
371	B
373	B
375	B
385	B

		371	B							377	B
		375	B								
		358		**348**		**AVG**				**374**	
		16		**28**		**DIFF**				**24**	
		352	Q	353	Q		348	QF			
		335	Q	345	Q		352	Q			
		371	Q	352	FQ		365	Q			
		373	Q	347	FQ		364	FQ			
				335	FQ						
		358		**346**		**AVG**	**357**				
		16		**26**		**DIFF**	**26**				
		348	H	345	H					375	H
				360	H					372	H
				343	H					380	H
				348	H						
				348	H						
				335	H						
				366	H						
				349		**AVG**				**376**	
				29		**DIFF**				**26**	

APPENDIX C: *ASPECT RATIO RAW DATA*

Raw data collected from thin sections. Used to calculate aspect ratios as summarized in Table 3.

Sample	**KK92.2**											
Orientation	**XZ plane □ to foliation**											
Mineral Measured (mm)	**Feldspar**				**Plagioclase Feldspar**				**Quartz**			
Plane	Grain Style	X	Z	Rxz = x/z	Grain Style	X	Z	Rxz = x/z	Grain Style	X	Z	Rxz = x/z
	A	0.98	0.64	1.53	F	3.60	1.36	2.65		2.70	0.26	10.38
	AB	2.10	0.68	3.09		0.56	0.30	1.87		1.80	0.34	5.29
		1.38	0.56	2.46		0.68	0.24	2.83		0.94	0.26	3.62
		0.38	0.16	2.38		0.58	0.20	2.90		2.24	0.40	5.60
		0.64	0.38	1.68		1.96	0.70	2.80		2.00	0.40	5.00
	B	1.52	0.56	2.71		2.50	1.30	1.92		1.40	0.26	5.38
	AB	3.16	1.06	2.98		0.70	0.50	1.40		2.24	0.48	4.67
	A	0.92	0.52	1.77		0.52	0.20	2.60		2.40	0.34	7.06
	AB	3.00	1.06	2.83						2.16	0.20	10.80
	AB	3.52	1.06	3.32						1.10	0.16	6.88
	B	2.00	0.56	3.57						1.68	0.24	7.00
	B	1.30	0.44	2.95						2.30	0.17	13.53
	VERY B	4.00	1.50	2.67						1.40	0.18	7.78
		1.70	0.56	3.04						1.92	0.28	6.86
		0.80	0.50	1.60						2.48	0.16	15.50
	F	0.96	0.40	2.40						2.00	0.24	8.33
	A	2.00	0.90	2.22						1.38	0.20	6.90
		1.28	0.78	1.64						0.72	0.20	3.60
	AB	2.56	1.30	1.97						0.78	0.20	3.90
	AB	1.40	0.70	2.00						2.24	0.12	18.67
	FB	1.40	0.56	2.50						1.16	0.32	3.63
	F	2.40	0.90	2.67						2.00	0.24	8.33
	FB	2.66	0.80	3.33						1.00	0.20	5.00
	AFB	3.06	1.06	2.89						1.90	0.34	5.59
	B	1.52	0.70	2.17						2.00	0.32	6.25
		2.66	1.44	1.85						1.18	0.28	4.21
		1.96	0.88	2.23								
		1.24	0.44	2.82								
		0.56	0.40	1.40								
		0.58	0.20	2.90								
		0.98	0.34	2.88								
Harmonic Mean:				**2.32**				**2.23**				**6.05**
Arithmetic Mean:				**2.47**				**2.37**				**7.30**
Standard Deviation:				**0.59**				**0.56**				**3.76**

Sample	KK92.1											
Orientation	YZ // TO LINEATION											
Mineral Measured (mm)	Feldspar				Plagioclase Feldspar				Quartz			
Plane	Grain Style	Y	Z	Ryz = Y/Z	Grain Style	Y	Z	Ryz = Y/Z	Grain Style	Y	Z	Ryz = Y/Z
	F	2.36	1.64	1.44		2.44	0.98	2.49		1.00	0.40	2.50
	F	1.60	0.83	1.93		0.60	0.40	1.50		0.80	0.30	2.67
	FB	1.84	0.92	2.00		0.64	0.30	2.13		4.00	0.70	5.71
	FB	5.00	2.70	1.85		2.00	0.60	3.33		2.60	0.48	5.42
	FB	5.72	2.00	2.86		0.44	0.18	2.44		1.24	0.18	6.89
		1.70	0.70	2.43		0.56	0.20	2.80		2.00	0.58	3.45
	B	3.80	1.84	2.07		0.98	0.48	2.04		1.50	0.30	5.00
		0.80	0.38	2.11		0.30	0.18	1.67		0.50	0.16	3.13
	F	1.56	0.43	3.63		4.00	1.80	2.22		1.20	0.18	6.67
		3.76	1.36	2.76		0.72	0.34	2.12		0.80	0.20	4.00
		0.80	0.40	2.00		0.60	0.26	2.31		1.50	0.18	8.33
		1.20	0.48	2.50		0.50	0.20	2.50		1.00	0.10	10.00
		1.60	0.62	2.58		0.64	0.30	2.13		0.80	0.14	5.71
		2.00	1.25	1.60		0.48	0.18	2.67		1.00	0.18	5.56
		1.70	0.70	2.43		0.70	0.26	2.69		1.28	0.26	4.92
	F	2.30	1.00	2.30								
		0.80	0.61	1.31								
		1.60	0.58	2.76								
		2.10	0.80	2.63								
	FB	2.00	0.75	2.67								
		1.10	0.40	2.75								
	B	1.90	0.90	2.11								
	FB	1.66	0.81	2.05								
	F	1.18	0.53	2.23								
	F	1.52	0.68	2.24								
Harmonic Mean:				**2.18**				**2.25**				**4.59**
Arithmetic Mean:				**2.29**				**2.34**				**5.33**
Standard Deviation:				**0.501**				**0.454**				**2.086**

Sample	KK102.2														
Orientation	XZ ⊥ TO FOLIATION														
Mineral Measured (mm)	Feldspar			Plagioclase Feldspar			Quartz			Biotite			Hornblende		
Plane	X	Z	Rxz = X/Z	X	Z	Rxz = X/Z	X	Z	Rxz = X/Z	X	Z	Rxz = X/Z	X	Z	Rxz = X/Z
	2.50	1.10	2.27	4.00	2.20	1.82	1.30	0.30	4.33	0.94	0.40	2.35	2.00	0.40	5.00
	2.24	1.66	1.35	5.00	2.96	1.69	1.80	0.36	5.00	2.00	0.80	2.50	3.00	0.60	5.00
	2.90	1.16	2.50	2.40	1.40	1.71	2.54	0.70	3.63	1.00	0.20	5.00	3.40	1.50	2.27
	4.00	2.60	1.54	2.00	1.20	1.67	1.42	0.42	3.38	1.40	0.60	2.33	1.20	0.60	2.00
	1.46	0.78	1.87	0.66	0.22	3.00	3.70	0.50	7.40	1.60	1.00	1.60	1.50	0.70	2.14
	2.66	1.50	1.77	1.10	0.60	1.83	4.00	0.44	9.09	1.80	0.70	2.57	2.00	0.26	7.69
	0.76	0.40	1.90	4.00	2.60	1.54	2.72	0.80	3.40	0.90	0.20	4.50	2.00	1.30	1.54
	1.10	0.60	1.83	1.40	0.70	2.00	1.04	0.30	3.47	1.50	0.32	4.69	1.60	1.00	1.60
	0.88	0.50	1.76	3.20	1.80	1.78	3.08	0.64	4.81	1.40	0.60	2.33	1.40	0.50	2.80
	1.00	0.56	1.79	1.80	0.80	2.25	2.24	0.48	4.67	3.60	1.00	3.60	1.60	0.80	2.00
				1.20	0.70	1.71				2.00	0.60	3.33			
				2.68	1.68	1.60									
				1.60	0.78	2.05									
				5.80	4.00	1.45									
				0.86	0.46	1.87									
				1.68	0.68	2.47									
				0.76	0.40	1.90									
				2.50	1.40	1.79									
				1.68	0.72	2.33									
				1.84	0.90	2.04									
				1.60	1.20	1.33									
				1.84	0.90	2.04									
				1.20	0.76	1.58									
				0.72	0.30	2.40									
				1.30	0.56	2.32									
				2.20	1.00	2.20									
Harmonic Mean:			**1.81**			**1.88**			**4.44**			**2.81**			**2.46**
Arithmetic Mean:			**1.86**			**1.94**			**4.92**			**3.16**			**3.20**
Standard Deviation:			**0.33**			**0.37**			**1.90**			**1.14**			**2.03**

Sample	KK102.1														
Orientation	YZ // TO LINEATION														
Mineral Measured (mm)	Feldspar			Plagioclase Feldspar			Quartz			Biotite			Hornblende		
Plane	Y	Z	Ryz = Y/Z	Y	Z	Ryz = Y/Z	Y	Z	Ryz = Y/Z	Y	Z	Ryz = Y/Z	Y	Z	Ryz = Y/Z
	2.08	1.08	1.93	1.70	0.86	1.98	5.10	0.90	5.67	1.16	0.60	1.93	2.00	0.60	3.33
	2.34	1.20	1.95	3.40	1.70	2.00	2.00	0.56	3.57	1.40	0.50	2.80	0.80	0.40	2.00
	1.66	0.98	1.69	2.40	1.30	1.85	2.26	1.00	2.26	1.12	0.50	2.24	1.00	0.50	2.00
	1.12	0.56	2.00	3.84	2.46	1.56	0.98	0.20	4.90	0.50	0.22	2.27	0.60	0.30	2.00
	1.68	0.84	2.00	2.46	1.30	1.89	3.00	1.30	2.31	0.86	0.36	2.39	0.80	0.30	2.67
	0.60	0.30	2.00	3.30	1.70	1.94	1.10	0.26	4.23	1.40	0.72	1.94	1.00	0.40	2.50
	1.26	0.63	2.00	1.16	0.56	2.07	0.70	0.20	3.50	1.12	0.56	2.00			
	0.90	0.50	1.80	1.84	1.08	1.70	1.50	0.56	2.68	1.72	0.80	2.15			
	4.36	2.30	1.90	5.80	2.50	2.32	1.40	0.46	3.04	1.10	0.40	2.75			
	3.40	2.20	1.55	1.80	1.12	1.61	2.30	0.50	4.60	1.00	0.56	1.79			
	4.00	2.50	1.60	3.80	2.00	1.90	1.00	0.16	6.25	1.40	0.70	2.00			
	1.36	0.76	1.79	4.00	2.00	2.00	1.06	0.20	5.30	1.20	0.30	4.00			
	2.00	1.06	1.89	1.30	0.66	1.97	2.20	0.24	9.17	1.00	0.60	1.67			
	1.26	0.63	2.00	1.74	1.00	1.74	2.70	0.60	4.50	2.00	1.00	2.00			
	2.26	1.45	1.56	3.30	1.70	1.94	1.80	0.50	3.60						
	1.00	0.64	1.56	1.80	1.00	1.80	2.40	0.75	3.20						
	1.76	1.20	1.47	0.74	0.36	2.06	7.44	1.92	3.88						
	1.00	0.58	1.72	1.08	0.52	2.08	6.00	1.36	4.41						
	0.90	0.50	1.80	2.24	1.30	1.72	3.80	0.68	5.59						
	2.80	1.46	1.92	2.00	1.10	1.82	2.00	0.50	4.00						
	3.30	1.66	1.99	1.78	0.72	2.47	3.36	0.66	5.09						
	2.06	1.06	1.94	1.04	0.56	1.86	2.50	0.72	3.47						
	1.44	0.84	1.71	3.90	2.04	1.91	2.70	1.04	2.60						
	1.84	1.04	1.77	0.80	0.52	1.54	1.40	0.36	3.89						
				0.90	0.52	1.73	2.76	0.70	3.94						
				1.40	0.68	2.06	2.72	0.54	5.04						
				2.70	1.50	1.80	3.44	0.72	4.78						
				3.36	1.75	1.92	1.64	0.48	3.42						
							2.00	0.40	5.00						
							1.34	0.34	3.94						
							1.30	0.10	13.00						
Harmonic Mean:			**1.80**			**1.88**			**3.99**			**2.18**			**2.33**
Arithmetic Mean:			**1.81**			**1.90**			**4.54**			**2.28**			**2.42**
Standard Deviation:			**0.17**			**0.21**			**2.07**			**0.59**			**0.53**

Sample	KK115.1														
Orientation	XZ ⊥ TO FOLIATION														
Mineral Measured (mm)	Feldspar			Plagioclase Feldspar			Quartz			Biotite			Hornblende		
Plane	X	Z	Rxz = X/Z	X	Z	Rxz = X/Z	X	Z	Rxz = X/Z	X	Z	Rxz = X/Z	X	Z	Rxz = X/Z
	1.00	0.50	2.00	2.24	1.68	1.33	2.00	0.46	4.35	1.80	0.40	4.50	1.60	0.60	2.67
	1.68	1.28	1.31	1.50	0.60	2.50	2.26	0.45	5.02	0.40	0.08	5.00	0.50	0.26	1.92
	2.10	1.30	1.62	3.76	1.40	2.69	0.84	0.26	3.23	0.90	0.20	4.50	1.30	0.50	2.60
	1.50	0.80	1.88	4.36	2.00	2.18	3.00	0.50	6.00	1.10	0.12	9.17	1.80	0.60	3.00
	0.90	0.30	3.00	1.86	1.06	1.75	4.90	1.72	2.85	1.00	0.20	5.00	1.30	0.50	2.60
	2.50	1.10	2.27	2.44	1.40	1.74	2.64	0.76	3.47	1.20	0.20	6.00	2.30	0.80	2.88
	2.00	1.30	1.54	1.80	1.00	1.80	2.50	0.22	11.36	1.40	0.30	4.67	1.40	0.70	2.00
	0.80	0.44	1.82	5.80	2.40	2.42	6.84	0.90	7.60	0.80	0.20	4.00	1.30	0.46	2.83
	3.20	1.20	2.67	3.90	1.90	2.05	2.10	0.40	5.25	1.30	0.30	4.33	1.16	0.46	2.52
	1.90	1.00	1.90	2.00	1.00	2.00	1.60	0.20	8.00	2.00	0.58	3.45	1.80	0.90	2.00
	3.12	1.92	1.63	2.40	1.20	2.00				1.60	0.44	3.64	1.20	0.44	2.73
	0.56	0.30	1.87	4.00	2.60	1.54				0.70	0.10	7.00	1.50	0.62	2.42
	0.98	0.40	2.45	2.00	0.76	2.63				0.60	0.10	6.00	1.20	0.62	1.94
	0.88	0.46	1.91	3.36	1.00	3.36				0.60	0.14	4.29	1.60	0.60	2.67
	6.72	2.90	2.32	1.96	0.70	2.80				2.00	0.48	4.17	1.00	0.40	2.50
	2.44	1.04	2.35	1.00	0.72	1.39				0.80	0.26	3.08			
	1.50	0.80	1.88	2.70	1.40	1.93				0.70	0.20	3.50			
	3.80	2.36	1.61	1.68	0.76	2.21				0.60	0.20	3.00			
	1.70	0.80	2.13	0.86	0.56	1.54				1.00	0.16	6.25			
	1.56	0.60	2.60	3.40	1.76	1.93				1.12	0.33	3.39			
	1.60	0.90	1.78												
	1.40	0.80	1.75												
	1.80	0.70	2.57												
	3.84	1.44	2.67												
	3.10	1.36	2.28												
	1.40	0.76	1.84												
	3.12	1.40	2.23												
	2.86	1.80	1.59												
	2.76	1.80	1.53												
	1.80	1.20	1.50												
	0.76	0.36	2.11												
Harmonic Mean:			**1.94**			**1.98**			**4.81**			**4.38**			**2.43**
Arithmetic Mean:			**2.02**			**2.09**			**5.71**			**4.75**			**2.48**
Standard Deviation:			**0.42**			**0.52**			**2.64**			**1.52**			**0.36**

Sample	KK115.2														
Orientation	YZ // TO LINEATION														
Mineral Measured (mm)	Feldspar			Plagioclase Feldspar			Quartz			Biotite			Hornblende		
Plane	Y	Z	Ryz = Y/Z	Y	Z	Ryz = Y/Z	Y	Z	Ryz = Y/Z	Y	Z	Ryz = Y/Z	Y	Z	Ryz = Y/Z
	1.40	0.90	1.56	2.60	1.10	2.36	2.30	1.12	2.05	0.52	0.20	2.60	1.12	0.70	1.60
	0.80	0.50	1.60	2.50	1.20	2.08	2.20	0.75	2.93	0.78	0.20	3.90	1.20	0.48	2.50
	1.10	0.56	1.96	1.30	0.90	1.44	2.00	1.00	2.00	0.96	0.28	3.43	0.52	0.18	2.89
	2.00	0.80	2.50	2.00	1.10	1.82	2.80	0.60	4.67	0.68	0.20	3.40	1.20	0.32	3.75
	1.28	0.66	1.94	4.00	1.80	2.22	1.66	0.24	6.92	0.20	0.70	0.29	2.00	0.76	2.63
	4.80	2.40	2.00	4.00	2.60	1.54	0.90	0.24	3.75	0.84	0.30	2.80	1.68	0.60	2.80
	0.90	0.40	2.25	1.80	1.00	1.80	1.60	0.48	3.33	0.50	0.18	2.78	1.20	0.60	2.00
	0.80	0.44	1.82	1.80	0.90	2.00	1.52	0.24	6.33	1.20	0.48	2.50	1.04	0.28	3.71
	1.50	0.60	2.50	1.84	0.80	2.30	1.90	0.50	3.80	2.00	0.58	3.45	1.40	0.64	2.19
	1.70	1.00	1.70	3.24	2.20	1.47	1.72	0.56	3.07	0.80	0.24	3.33	4.00	2.06	1.94
	4.00	1.80	2.22	1.70	0.64	2.66	2.00	0.98	2.04	0.70	0.42	1.67	1.30	0.50	2.60
	0.90	0.44	2.05	1.80	1.00	1.80							0.80	0.50	1.60
	1.00	0.68	1.47	2.00	0.80	2.50							0.76	0.36	2.11
	5.20	3.12	1.67	4.40	2.20	2.00							2.00	0.88	2.27
	5.00	2.20	2.27	0.52	0.30	1.73							1.92	0.90	2.13
	2.00	1.00	2.00	1.60	0.72	2.22							1.60	0.78	2.05
	4.80	2.60	1.85												
	2.30	1.40	1.64												
	2.30	1.00	2.30												
	1.40	0.88	1.59												
	1.44	0.62	2.32												
Harmonic Mean:			**1.91**			**1.93**			**3.15**			**1.56**			**2.29**
Arithmetic Mean:			**1.96**			**2.00**			**3.72**			**2.74**			**2.42**
Standard Deviation:			**0.32**			**0.364**			**1.664**			**1.018**			**0.634**

Sample	KK158.1														
Orientation	XZ plane ⊥ to foliation														
Mineral Measured (mm)	Feldspar			Plagioclase Feldspar			Quartz			Biotite			Hornblende		
Plane	X	Z	Rxz = X/Z	X	Z	Rxz = X/Z	X	Z	Rxz = X/Z	X	Z	Rxz = X/Z	X	Z	Rxz = X/Z
	2.00	1.00	2.00	2.00	1.00	2.00	5.00	1.30	3.85	4.00	2.00	2.00	2.20	0.64	3.44
	2.50	1.20	2.08	1.90	0.80	2.38	2.00	0.35	5.71	2.80	0.90	3.11	2.60	0.83	3.13
	2.50	1.25	2.00	2.20	1.40	1.57	4.00	0.80	5.00	0.80	0.26	3.08	2.80	0.80	3.50
	1.00	0.52	1.92	1.70	0.90	1.89	2.00	0.20	10.00	2.00	1.00	2.00	1.24	0.28	4.43
	3.00	1.50	2.00	1.50	0.70	2.14	3.60	0.50	7.20	1.10	0.55	2.00	1.60	0.60	2.67
	1.60	0.80	2.00	4.00	2.10	1.90	4.30	1.00	4.30	1.00	0.18	5.56			
	2.40	0.90	2.67	6.00	3.28	1.83	2.00	0.20	10.00						
	2.40	1.20	2.00	1.20	0.60	2.00	2.20	0.22	10.00						
	1.00	0.50	2.00	1.80	0.70	2.57	4.80	0.80	6.00						
	0.90	0.45	2.00	2.20	1.20	1.83	3.00	1.00	3.00						
	0.98	0.48	2.04	3.10	1.50	2.07	2.00	0.26	7.69						
				3.00	1.00	3.00	2.30	0.40	5.75						
				2.20	1.40	1.57	2.10	0.44	4.77						
							1.70	0.50	3.40						
							###	2.00	5.00						
							1.80	0.30	6.00						
							1.40	0.20	7.00						
							1.20	0.26	4.62						
							2.40	0.50	4.80						
							9.90	2.00	4.95						
							2.00	0.24	8.33						
							2.00	0.44	4.55						
							2.00	0.12	16.67						
							2.00	0.48	4.17						
Harmonic Mean:			**2.05**			**2.00**			**5.47**			**2.58**			**3.34**
Arithmetic Mean:			**2.06**			**2.06**			**6.36**			**2.96**			**3.43**
Standard Deviation:			**0.20**			**0.40**			**2.99**			**1.38**			**0.65**

Sample	KK158.2											
Orientation	YZ // TO LINEATION											
Mineral Measured (mm)	Feldspar				Plagioclase Feldspar				Quartz			
Plane	Grain Style	Y	Z	Ryz = Y/Z	Grain Style	Y	Z	Ryz = Y/Z	Grain Style	Y	Z	Ryz = Y/Z
		1.50	0.90	1.67		1.02	0.60	1.70		2.00	0.56	3.57
		1.80	0.90	2.00		4.60	2.00	2.30		2.00	0.20	10.00
		3.60	1.70	2.12	F	4.00	1.90	2.11		3.00	0.90	3.33
		2.30	1.40	1.64		2.52	1.30	1.94		2.40	1.10	2.18
		1.80	1.00	1.80		0.70	0.44	1.59		3.00	0.90	3.33
		1.70	1.10	1.55		1.20	0.50	2.40		1.20	0.40	3.00
		1.90	1.10	1.73		1.40	0.80	1.75		1.48	0.58	2.55
						1.90	1.20	1.58		2.80	0.60	4.67
						1.00	0.36	2.78		3.00	0.40	7.50
						1.60	0.90	1.78		1.20	0.30	4.00
						3.20	1.00	3.20				
						0.80	0.50	1.60				
						1.70	1.00	1.70				
						1.60	1.00	1.60				
						1.80	0.80	2.25				
						2.50	1.60	1.56				
						1.60	0.80	2.00				
					FB	2.90	1.60	1.81				
						1.50	0.80	1.88				
					B	2.80	1.50	1.87				
						2.50	1.50	1.67				
					F	4.20	2.60	1.62				
Harmonic Mean:				**1.77**				**1.87**				**3.62**
Arithmetic Mean:				**1.79**				**1.94**				**4.41**
Standard Deviation:				**0.20**				**0.42**				**2.46**

REFERENCES CITED

Davis, GH. Reynolds, SJ. Structural Geology of Rocks and Regions. John Wiley & Sons, Inc. USA. Second Edition. 1996.

English, JM. Johnson, ST. Wang, K. 2003. Thermal modeling of the Laramide orogeny: testing the flat-slab subduction hypothesis. Earth and Planetary Science Letters; Vol. 214; Issues 3-4; p. 619-632.

Nourse, JA. 1989. Geological Evolution of Two Crustal Scale Shear Zones. California Institute of Technology; Thesis for the degree of Doctor of Philosophy.

Schultejann, PA. 1984. The Yaqui Ridge Antiform And Detachment Fault Mid-Cenozoic Extensional Terrane, West of the San Andreas Fault. Tectonics; Vol. 3; No. 6; P. 677-691.

Sibson, RH., 1977. Fault rocks and fault mechanisms. Geology; Vol. 133; p. 191-213.

Silver, LT. 1991. Daughter-parent isotope systematics in U-Th-bearing igneous accessory mineral assemblages as potential indices of metamorphic history: A discussion of the concept. Stable Isotope Geochemistry; Special Publication; No. 3.

Simpson, C., Schmid, SM., 1983. An evolution of criteria to deduce the sense of movement in sheared rocks. Geological Society of America Bulletin; Vol. 94; p. 1281 – 1288.

Simpson, C. 1984a. Borrego Springs – Santa Rosa mylonite zone: A Late Cretaceous west-directed thrust in Southern California. Geology; Vol. 12; p. 8-11.

Simpson, C., 1984b. Deformation of granitic rocks across the brittle-ductile transition. Journal of Structural Geology.

Simpson, C., 1986. Fabric Development in Brittle-to-Ductile Shear Zones. Pageoph; Vol. 124; Nos ½.

Thompson, CN. Girty, GH. 1994. Early Cretaceous intra-arc ductile strain in Triassic-Jurassic and Cretaceous continental margin arc rocks, Peninsular Ranges, California. Tectonics; Vol. 13; No. 5; p. 1108-1119.

Wetmore, PH, Herzig, C, Alsleben, H, Sutherland, M, Schmidt, KL, Schultz, PW, and Paterson, SR. 2003, Mesozoic tectonic evolution of the Peninsular Ranges of southern and Baja California, *in* Johnson, SE, Paterson, SR, Fletcher, JM, Girty,GH, Kimbrough, DL, and Martin-Barajas, A, eds., Tectonic evolution of northwestern Mexico and the southwestern USA: Geological Society of America Special Paper 374, p. 93-116.